Received: 29 November 2022 | Revised: 19 April 2023 | Accepted: 22 April 2023

DOI: 10.1002/eqe.3906

RESEARCH ARTICLE

WILEY

Triaxial shake table testing of an integrated low-damage building system

Stefano Pampanin[1] | **Jonathan Ciurlanti**[1] | **Simona Bianchi**[1] | **Daniele Perrone**[2] | **Gabriele Granello**[3] | **Michele Palmieri**[4] | **Damian N. Grant**[5] | **Alessandro Palermo**[3] | **Alfredo Campos Costa**[6] | **Paulo X. Candeias**[6] | **António A. Correia**[6]

[1]Sapienza University of Rome, Rome, Italy

[2]University School for Advanced Studies IUSS, Pavia, Italy

[3]University of Canterbury, Christchurch, New Zealand

[4]Arup, Amsterdam, The Netherlands

[5]Arup, London, United Kingdom

[6]Laboratório Nacional de Engenharia Civil LNEC, Lisbon, Portugal

Correspondence
S. Bianchi, Delft University of Technology, Delft, The Netherlands.
Email: s.bianchi@tudelft.nl

Present address
Jonathan Ciurlanti, ARUP, Amsterdam, Netherlands
Simona Bianchi, Delft University of Technology, Delft, The Netherlands
Daniele Perrone, University of Salento, Lecce, Italy
Gabriele Granello, Open Systems Lab, Open Systems Lab, St. Ives, United Kingdom

Funding information
European Union's Horizon 2020 research and innovation programme

Abstract

Lessons from recent earthquakes have provided a tough reality check of the traditional seismic design approach and technologies, highlighting the urgent need for a paradigm shift of performance-based design criteria and objectives toward low-damage design philosophy and technologies for the whole building system. Modern society is asking for "earthquake proof" resilient buildings that are able to withstand seismic events without compromising their functionality. The EU-funded SERA (Seismology and Earthquake Engineering Research Infrastructure Alliance for Europe Project) project discussed in this paper provided the opportunity to develop and validate within the European context an integrated seismic low-damage prototype, including main structure and non-structural elements, for the next generation of high-performance buildings. This paper presents an overview of the research, involving three-dimensional shake table tests of a two-storey 1:2 scaled timber-concrete post-tensioned dissipative low-damage structure "dressed" by earthquake-resistant gypsum/masonry partitions and glass/concrete facades. Specimen details, construction and assembly phases, test setup, and experimental results are discussed. After many cycles of input motions at increasing levels of seismic intensity (higher than Collapse Prevention Limit State), the integrated building system exhibited a very high seismic performance. The experimental campaign carried out at the National Laboratory of Civil Engineering in Lisbon confirmed the unique potential of low-damage technologies and the opportunity for their widespread implementation into design practice.

KEYWORDS
experimental tests, low-damage, non-structural elements, post-tensioned frames and walls, seismic performance, timber-concrete structure

NOVELTY

The main contributions of the paper to the field are:

- Demonstration of the high seismic potential of integrated structural (frames, walls) and non-structural (facades, partitions) low-damage building configurations through 3D shake table testing (in-plane horizontal and vertical directions).
- Indications on the specimen design, testing set-up, and protocol for the replicability of the low-damage solutions and testing implementation.
- The advantage of applying low-damage connection details for the overall building system, particularly by providing an assessment of the experimental results and damage mechanisms, as well as by suggesting detailing improvements for future applications.

1 | INTRODUCTION: SEISMIC-RESISTANT VERSUS EARTHQUAKE-PROOF

The significant socio-economic impacts of recent earthquake events in developed countries have clearly and critically highlighted the great mismatch between societal expectations over the reality of engineered buildings' seismic performance. The engineering concept embodied with a code-based design approach defines an earthquake-resistant building as a structure capable of sustaining a design level earthquake with extensive—often not repairable—damage to structural and non-structural elements, with the main target being the Life-Safety of the building occupants. This is apparently far from the expectations of the general public who would rather expect to be provided with an actual "earthquake-proof" structure.[1,2]

The actual performance of modern building stock (Figure 1A) has come as a shocking surprise to the general population. On the one hand, a better communication between technical professionals and stakeholders would help in clarifying and disclosing to the wider public what accepted and targeted performance levels are built into a design code, itself to be considered as a "minimum" (not a maximum nor target) standard. On the other hand, the Earthquake Engineering community is challenged with the complex task to "raise the bar" by shifting the targeted performance goals[3] from the typically accepted Life-Safety level to a more appropriate and needed Damage-Control level in a major earthquake ground motion, all this without (significantly) increasing the cost of construction.[4] These increased expectations and associated new goals would require a significant paradigm shift in terms of performance-based seismic design, which can be

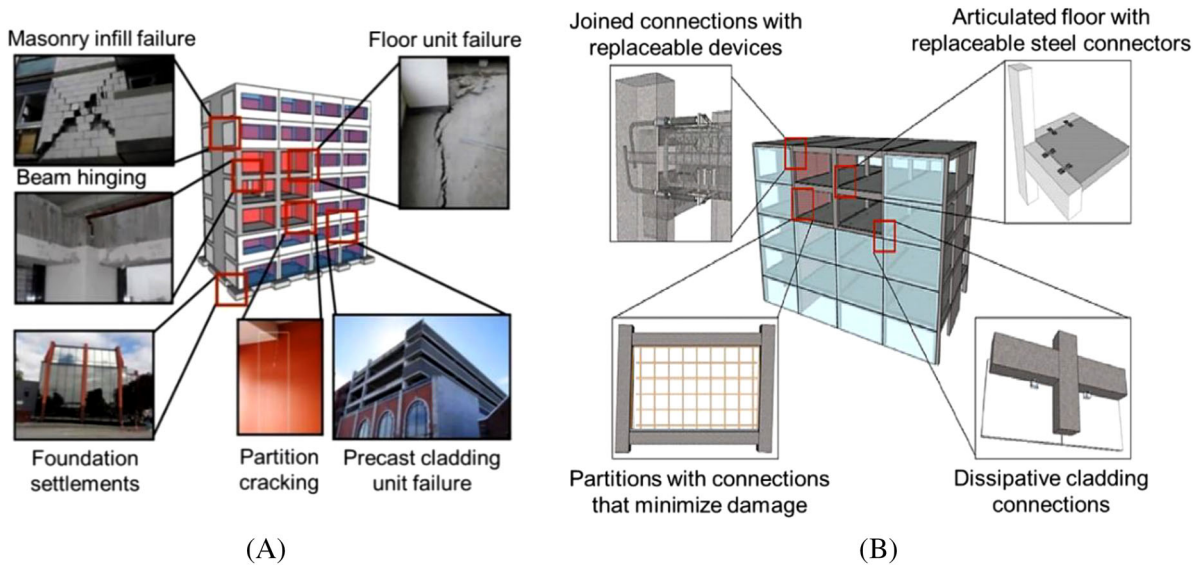

FIGURE 1 (A) Damage to a modern building system; (B) concept of integrated low-damage building system.[5]

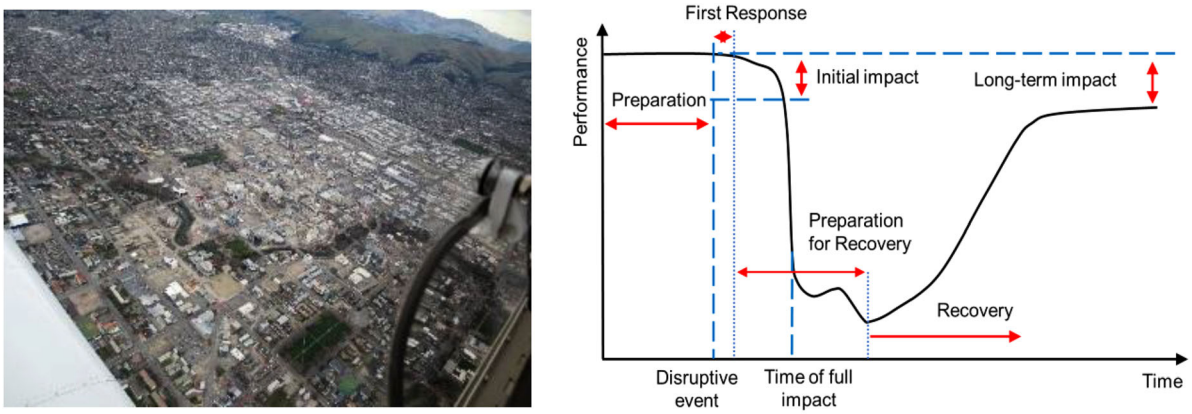

FIGURE 2 (A) Aerial view of Central Building District in Christchurch in the aftermath of the 2010–2011 Earthquake Sequence with entire blocks being demolished (Photo courtesy of Kam Weng); (B) concept of Resilience (adapted from Sheffi and Rice[10]).

accomplished by the development and/or further refinement of design methodologies as well as of high seismic-performance and cost-effective technologies for the whole building system, including the load-bearing structure, foundation systems, and non-structural elements (Figure 1B).

This paper presents an overview, with key results and outcomes, of an EU-Funded SERA (Seismology and Earthquake Engineering Research Infrastructure Alliance for Europe Project) Project titled "*(Towards the) Ultimate Earthquake Proof Building System: development and testing of integrated low-damage technologies for structural and non-structural elements*."[6] The SERA project (2017–2020) aimed to reduce the risk posed by natural and anthropogenic earthquakes based on innovative research and development projects, by providing access to experimental facilities in Europe and promoting multi-disciplinary science to improve understanding of earthquake occurrence. Within the SERA framework, the project described in this paper focused on the development and experimental validation of an integrated low-damage building system prototype, two-storey 1:2 scaled, including low-damage solutions for both the structural skeleton and the non-structural elements for the next generation of high-performance resilient buildings.

2 | TARGETING COMMUNITY RESILIENCE

Recent earthquake disasters have reinforced the idea that traditional design philosophies currently implemented through standards in the OECD countries are effective at preventing building collapses and loss of life, but in many cases lead to significant damage that may not be feasible to repair (Figure 2A). Building safer and more resilient communities should be and is eventually being recognized as the overarching goal of risk reduction policies and practices. The concept of resilience is generally related to the capacity to "bounce back" within a recovery time after absorbing the impact of an external event. This is shown in Figure 2B that presents a resilience curve (functionality vs. time) and the multiple phases involved before and after a disruptive event occurs. When dealing with seismic resilience, the concept is much wider than the evaluation of the seismic performance of a building through the evaluation of drift ratios and acceleration parameters, and is even broader than the evaluation of direct and indirect losses (as defined according to the Performance-Based Earthquake Engineering Framework,[7,8]). A general framework to define, quantitatively measure and enhance the seismic resilience of communities was initially proposed by Bruneau et al.,[9] in an attempt to support decision-makers to assess the progress made via alternative top-down or bottom-up practices and policies toward this ultimate goal of seismic risk reduction. Evidently, targeting a more damage-resistant or impact-resilient built environment, including structures and infrastructures, would represent a key and more tangible step towards the goal of building community resilience. This would score highly against two out of the three measures of resilience suggested in Bruneau et al.,[9] namely "*Reduced Failure Probability*" and "*Reduced Time to Recovery*," whilst the "*Reduced Consequences*" from failures would be more related to the overall structure/infrastructure system and associated intra and inter-dependencies.

FIGURE 3 Test Specimen configurations; (A) *Skeleton Building*; (B) *Option 1* (internal partitions) and (C) *Option 2* (integrated building system).

3 | THE NEXT GENERATION OF INTEGRATED LOW-DAMAGE BUILDINGS

Within this framework of seismic risk reduction and community resilience enhancement, the next crucial step in performance-based seismic design should more explicitly focus on the development of an integrated approach involving all aspects of the design framework, including design procedures as well as technological solutions for engineers and stakeholders to control the performance and damage of buildings. To this end, large-scale shake table tests (uni- or bi-directional) have been conducted on low-damage structures to provide evidence on their seismic potential. For instance, Henry et al.[11] performed experiments on a two-storey low-damage concrete structure consisting of post-tensioned rocking walls and incorporating a range of alternative energy dissipation devices; Newcombe et al.[12] tested a two-storey post-tensioned timber building under quasi static cyclic testing up to a design drift level of 2%; Mugabo et al.[13] tested a two-storey structure with Cross-Laminated Timber walls with U-shaped steel flexural plate energy dissipators. Although these experiments proved the high-performance of low-damage structural systems under increasing levels of shaking, they did not involve testing on integrated structural/non-structural building systems. On the other hand, large-scale experiments have been carried out on non-structural components such as rocking and dissipative precast concrete cladding panels [e.g.,[14,15]], innovative plasterboard partition walls [e.g.,[16–18]] and rocking masonry walls [e.g.,[19,20]]. These tests aimed at proving the efficacy of including cost-affordable low-damage detailing relying on sliding, rocking mechanisms, and dissipative connections to improve the performance of vertical architectural components.[21] Due to the need for investigating integrated structural/non-structural systems, a first low-damage prototype building was designed and tested through uniaxial shake table tests at the University of Canterbury.[5] The Test Specimen was a two-storey 1:2 scale concrete frame building consisting of a (unbonded) post-tensioned rocking frame with external replaceable *Plug&Play* dissipaters[22,23] and incorporating an articulated floor solution, low damage drywall infills and concrete facades. Details are similar to what is shown in Figure 1B. The specimen was tested under different configurations of structure plus building envelope (drywall partition, concrete facade), and subjected to over 400 earthquake ground motions of different intensity levels (up to Peak Ground Acceleration, PGA, equal to 0.7 g), with no evident structural and non-structural damage. Following the same objective, the ongoing (currently at the experiment design phase) Robust Building Systems, ROBUST, project[24] aims at enhancing the seismic resilience of buildings by introducing and validating low-damage concepts for both structural and non-structural elements, with a particular focus on steel structures.

As a further development of the 2014 research[5] and as part of a Horizon 2020 European-funded SERA (Seismology and Earthquake Engineering Research Infrastructure Alliance for Europe Project) project titled "*(Towards the) Ultimate earthquake proof building system: development and testing of integrated low-damage technologies for structural and non-structural elements"* and coordinated by Sapienza University of Rome,[6] shake table tests were carried out on a 1:2 scale two-storey two-bay low-damage building system consisting of a self-centering and dissipative timber-concrete structural skeleton[25–28] with external replaceable *Plug&Play* dissipaters and high-performance or damage-resistant architectural elements (partitions and facades). The frames have timber beams and concrete columns to maximize the overall structural performance of the lateral load building, reducing the weight and the overall embedded carbon footprints, while the walls were built with Cross Laminated Timber (CLT) and timber drag-beams. Three different specimen configurations (Figure 3) were tested at the Laboratório Nacional de Engenharia Civil (LNEC) in Lisbon. Three alternative testing phases were identified for these tests:

- Phase 1: The *Skeleton Building* system, consisting of unbonded post-tensioned rocking dissipative frames in the longitudinal directions, with glue-laminated (Glulam) timber beams and precast concrete columns, and unbonded post-tensioned rocking-dissipative low-damage CLT walls in the transverse direction. As discussed later, the specimen had a Timber-Concrete Composite (TCC) flooring system at the first level and a Pre-stressed Timber-Concrete flooring system (3PT) at the second level.
- Phase 2: A first configuration of non-structural elements (*Option 1*), consisting of fiber-reinforced gypsum partitions built on the first floor in both structural directions;
- Phase 3: A second configuration of non-structural elements (*Option 2*), consisting of two facade systems, namely spider glazing curtain walls and Glass Fiber Reinforced Concrete (GFRC) precast claddings and an internal low-damage masonry infill wall.

This paper provides an overview of the overall SERA research project focusing on design procedure, specimen construction details, testing setup and protocol, and experimental results. More information on the structural details—from design to manufacturing—and analytical versus numerical versus experimental response of the specimen can be found in Ciurlanti et al.,[29] while the construction, seismic response and performance evaluation of the non-structural elements is discussed in Bianchi et al.[30]

4 | DESIGN AND CONSTRUCTION DETAILS OF THE TEST SPECIMEN

4.1 | Displacement-based seismic design

The Test Specimen was designed considering a full-scale building prototype with typical structural dimensions of an inner core of multi-storey commercial buildings, as well as ensuring the specimen could fit within the size and maximum payload capacity of the shake table at LNEC. Considering these restraints for the Test Specimen (the scaled building), a Prototype Building (the unscaled building) was initially designed as a two-storey structure with two seismic resistant unbonded post-tensioned timber-concrete frames in the longitudinal direction and two unbonded post-tensioned timber walls in the transverse direction. The Prototype Building footprint (column center-to-center) was 11.36 m × 10.4 m with 5.68 meters bay length in the frame direction, 10.4 meters bay length in the wall direction (total footprint of 11.96 m × 10.8 m) while the inter-storey height was 3.4 m. The Cauchy-Froude similitude of constant stress and constant acceleration was then applied to determine the configuration of the 1:2 scaled *Skeleton Building*. The similitude law allows a comparison of seismic behavior between the full-scale prototype and the reduced mock-up through a control of material densities, in order to reproduce the same working state as the prototype.[31] Following the Cauchy-Froude similitude law, additional masses were therefore identified to simulate the required increase in density due to the scaling approach (8.6 tons for the first level, 7.2 tons for the second level).

The seismic design of the specimen (Figure 4) was carried out following a direct displacement based design (DDBD) procedure[32,33] for an Importance Level 2 building (i.e., ordinary residential and commercial) located in a high seismic region (PGA = 0.353 g, soil type C, with the design spectrum defined according to the Italian Code[34]). The target maximum inter-storey drift ratios for a 475-year return period earthquake intensity were 1.20% and 1.15% in the frame and wall directions, respectively. The selection of the design drift ratio was mostly influenced by material verifications and construction feasibility. In the frame direction, the drift value was indeed limited by the high number of components resisting the seismic action and the construction feasibility of the dissipator sections. In the wall direction, the design drift value was instead limited by cracking verifications for the timber material (CLT C24). The post-tensioned rocking-dissipative systems were designed considering a re-centring ratio, λ (i.e. = M_{pt}/M_s, the re-centring moment contribution M_{pt} divided by the dissipative moment contribution M_s) equal to 1.25. Table 1 summarizes the key DDBD design parameters. As mentioned above, a detailed description of the design and dimensioning of the structural members can be found in Ciurlanti et al.[29]

4.2 | Structural details

The low-damage connections were designed considering the internal actions (shear, bending moment, axial force) and rotations obtained from the DDBD procedure through equilibrium approaches and methods provided by the NZCS

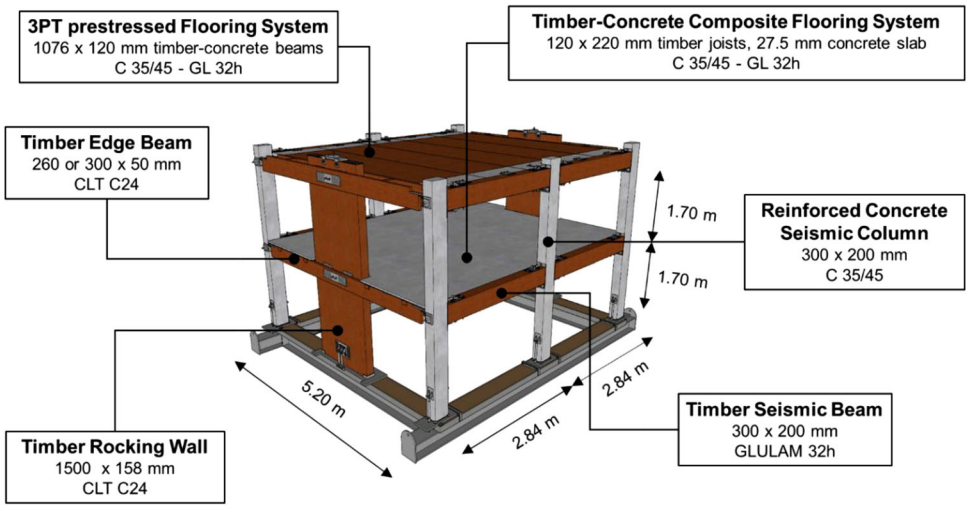

FIGURE 4 Test Specimen (*Skeleton Building*) details and dimensions.

TABLE 1 Direct displacement based design parameters of the Test Specimen.

Parameter	Frame direction	Wall direction
Design inter-storey drift θ_d [%]	1.20	1.15
Design displacement Δ_d [mm]	32.97	31.62
Effective mass m_e [t]	28.86	26.86
Effective height H_e [m]	2.75	2.75
Equivalent viscous damping ξ_{eq} [%]	13.39	14.69
Effective period T_e [s]	0.51	0.50
Effective stiffness K_e [kN/m]	4086.09	4265.15
Base shear V_b [kN]	134.70	134.88

PRESSS Design Handbook[32] for concrete elements and the STIC Design Guidelines[35] for timber components. Different typologies of post-tensioning systems were chosen for both frame and wall directions, namely 1/2″ 7-wire strands and 3/8″ 7-wire strands were selected for the seismic beams at the first and the second floor, respectively, while 18WR fully threaded post-tensioned bars were selected for the rocking timber walls. External *Plug&Play* dissipaters were specifically designed (fuse diameters and length) for each connection typology to achieve the correct amount of structural damping considered during the design phase, as per specifications provided by Sarti et al.[23] The dissipaters were obtained from necking-down 16 or 20 mm mild steel bars (from 16 to 6.8/8.8 mm for the beam dissipaters, from 20 to 14/15.6 mm for the column dissipaters, from 16 to 11 mm for the wall dissipaters). The dissipator anchorage in the column consisted of a coupling nut providing a robust screwed connection with an internal rebar, while a steel assembly was specifically fabricated to bolt the dissipator on the beam (Figure 5A). The anchorages were designed to locate the dissipators 30 mm far from the beam face, allowing them to be easily replaced and ensuring no undesired interaction with the rocking motion. For the connection of both columns and walls to the foundation, the dissipaters were screwed into welded couplers or directly bolted on the steel foundation plate, while a steel assembly was created to connect the dissipaters to the column/wall base (Figure 5B,C). Finally, regarding the post-tensioned wire strands and the post-tensioned threaded bar, a specific anchorage system was built on the corner columns and on the top and bottom of the timber wall/steel foundation (Figure 5D,E).

All the steel plates, bolts/screws/nails, and welding in the hybrid connections were verified by applying formulations from international codes (Eurocode 8, Italian NTC 2018,[34] and Standards New Zealand). Furthermore, many other structural details were included in order to provide the correct functionality to the overall system; that is, (1) to properly connect the foundation plates of columns and walls to the steel foundation available in the laboratory, (2) for positioning the seismic, edge and central beams, (3) to connect the edge (sandwich) beams to the wall by means of a pinned connection as well as to the lateral concrete columns, (4) for positioning the two flooring systems, and (5) to connect the floors to the lateral seismic resistant systems, thus allowing an appropriate transfer of forces to the structure.

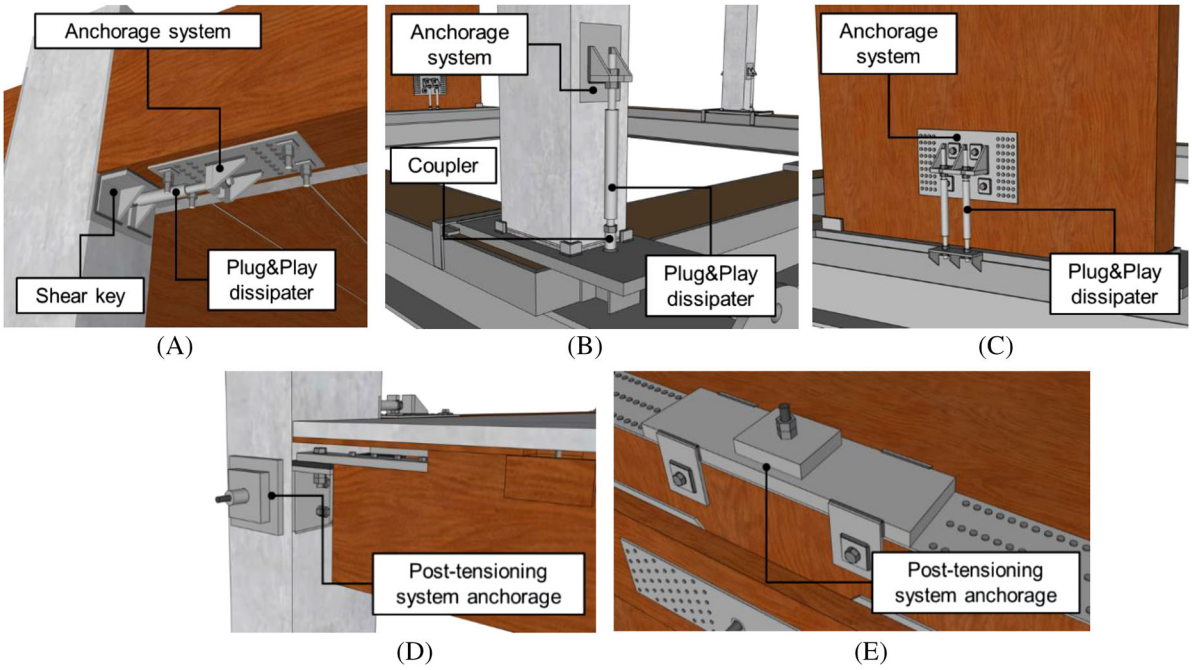

FIGURE 5 Construction details: (A) beam-column bottom connection (frame direction); (B) column-base; (C) wall-base connection; (D) beam-column top connection (wall direction); (E) wall-top connection.

Regarding the flooring systems, the first level was a Timber-Concrete Composite (TCC) floor (Figure 6A,C) designed following the STIC guidelines[35] and AS/NZS 1170 series[36] using a deflection control value of 1/300 of the span. The floor consisted of 120 × 220 mm timber joists, 12.5 mm plywood, and 27.5 mm concrete slab. Reinforcing bars were designed and introduced in the concrete slab to provide a correct diaphragm action to the floor. The second level was a 3PT timber-concrete floor[37] (Figure 6B,D) composed of 1076 × 120 mm prestressed timber-concrete beams.

4.3 | Non-structural details

The non-structural elements, apart from the low-damage masonry partition wall fully designed according to the design indications provided by Tasligedik and Pampanin,[20] were provided by the industry suppliers and their details were discussed and amended to be adapted to the dimensions and details of the main structure in order to develop a low-damage solution. This aligned with the objective of defining an integrated structural/non-structural building system to be easily implemented within the current construction practice. A detailed description of the non-structural detailing can be found in Bianchi et al.,[30] while a general overview is provided below.

Concerning the partitions tested during the second experimental phase (*Option 1*), the system consisted of two orthogonal walls: a 5 m long wall with openings in the wall direction and a 2.5 m long monolithic wall in the frame direction. These walls comprised steel sub-frames (with lateral gaps to the main structure) covered by fiber-reinforced ceramic gypsum panel. During the third testing phase *(Option 2)*, this system was demolished to be substituted by an unreinforced masonry partition with low-damage detailing, that is, 90 mm thick rocking vertical panels built inside an internal steel frame with specific details as described in the following section. Two types of facades were introduced to cover the structural skeleton: Glass Fiber Reinforced Concrete (GFRC) precast claddings in the longitudinal direction and spider glazing facades in the transverse direction. The precast cladding system consisted of 15 mm thick GFRC panels with a central opening. The panels were realized by means of a spray mix system of a cement-based composite material reinforced with alkali-resistant glass fibers. The external cladding was then connected through stirrups to a steel frame (with same overall dimensions) which, in turn, was attached to the structural members using two restraint anchorages at the bottom and two sliding connections at the top (Figure 7A–C). Spider glazing walls were composed of 10 + 1.52PVB + 10 mm laminated glass panels fixed to the structural skeleton by steel assemblies specifically designed (Figure 7D,E). The facade comprised articulated screws consisting of ball joints inserted

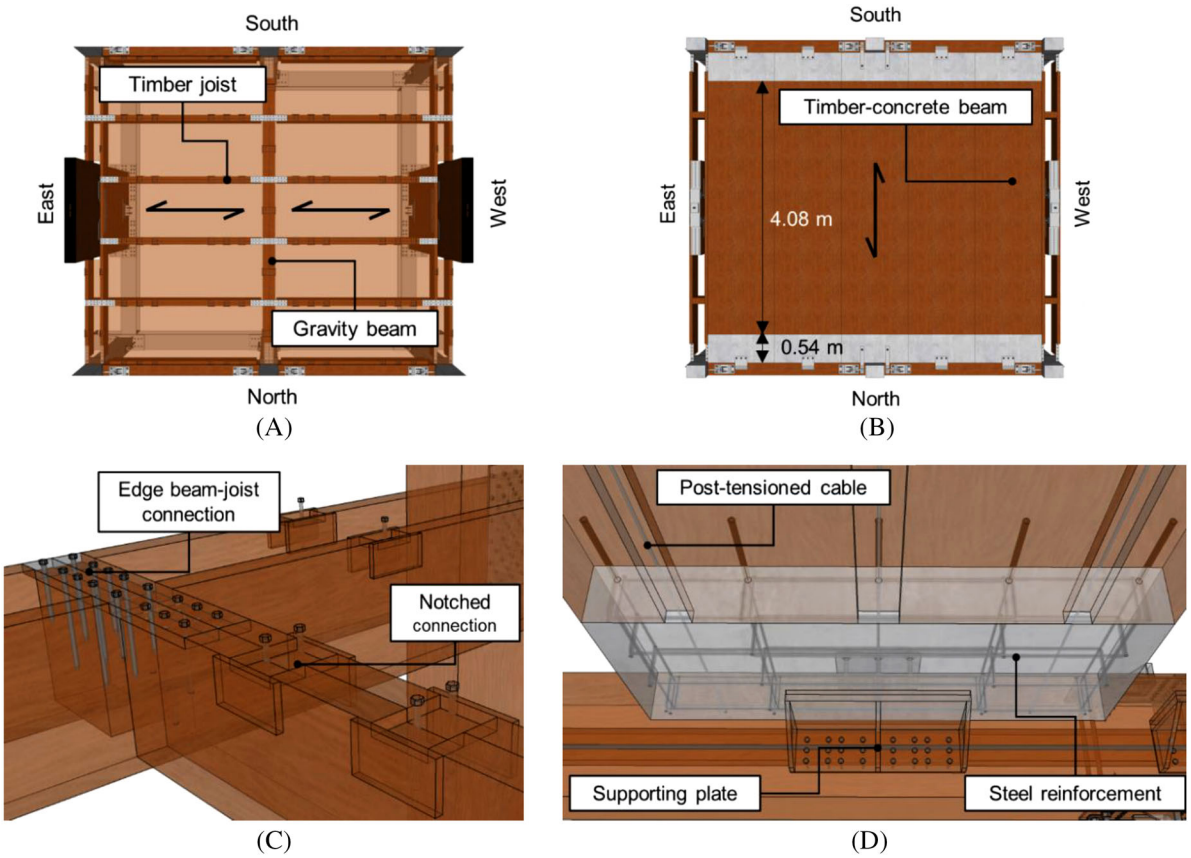

FIGURE 6 Plan views and details of: (A–C) Timber-Concrete Composite flooring system; (B–D) 3PT prestressed flooring system.

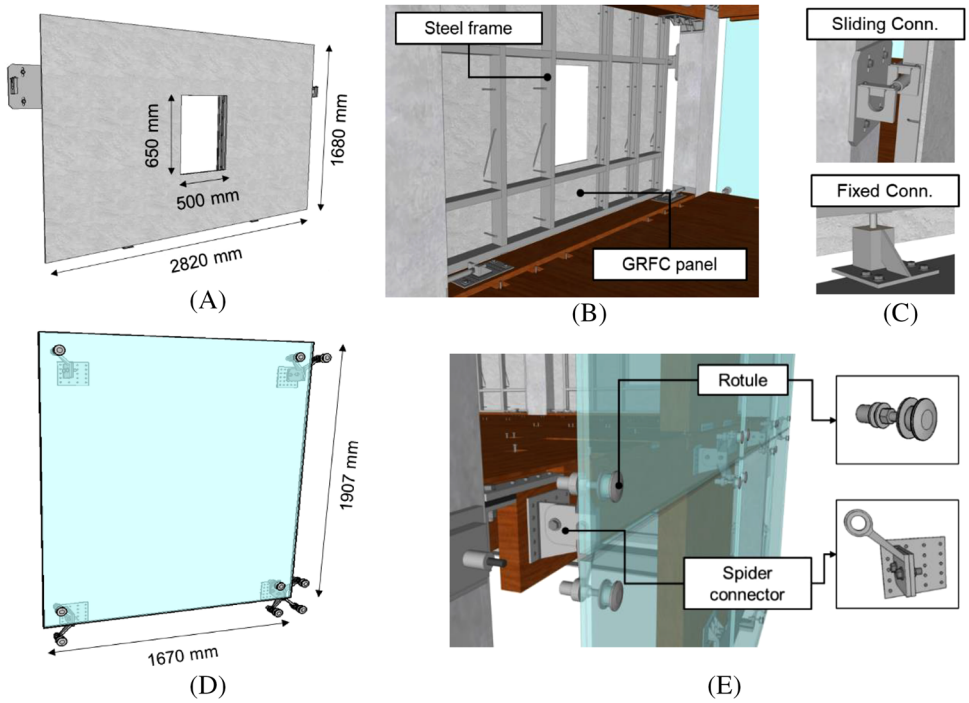

FIGURE 7 Rendering of the facades; (A) GFRC panel dimensions; (B) steel frame of a GRFC precast cladding; (C) sliding/restraint cladding-structure connections; (D) glass panel dimensions; (E) detail of the ball joint-spider connector-plate assembly of the glazed facade.

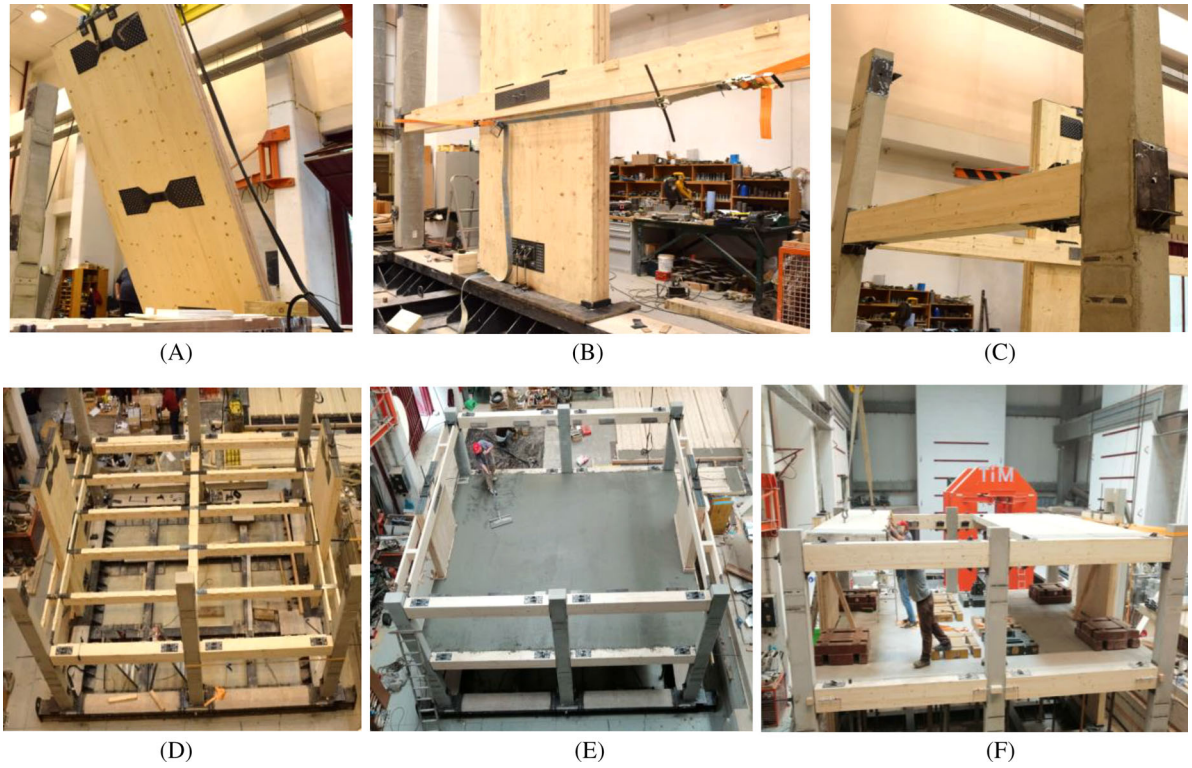

FIGURE 8 Construction phases of the *Skeleton Building*: (A) erection of the timber walls; (B) positioning of the edge transverse beams; (C) of the seismic longitudinal beams; (D) assembly of the timber joists; (E) casting of the concrete slab; (F) assembly of the second building floor.

within holes into the glass panels and bolted to spider connectors, in turn, connected to steel plates on the structural system.

5 | MANUFACTURING AND CONSTRUCTION OF THE TEST SPECIMEN

A consortium of Italian manufacturers was involved in the research project to supply the specimen components, fully fabricated in Italian plants and then transported by truck to Lisbon. The only components directly built in the laboratory by a local contractor were the infill clay brick masonry wall and the in-situ concrete parts of the flooring systems.

The *Skeleton Building* was entirely assembled off the shake table on the steel foundation available at LNEC. This typology of buildings is in fact conceived as a sort of "Lego" system, easy to be assembled and rapid to be constructed/erected with significantly reduced construction time when compared to traditional structures. The assembly of the system involved different phases, partly shown in Figure 8. More specifically: (a) the vertical components (reinforced concrete columns, CLT walls) were lifted and positioned on their steel plates fixed to the existing steel foundation; (b) the horizontal components in the wall direction (edge beams and central beam) were craned and positioned on their sitting plates and connected through slotted connections that transfer shear but allows for vertical wall displacements; (c) the seismic longitudinal beams were lifted and positioned on their steel corbels welded to the lateral plate embedded into the concrete columns. For the construction of the TCC floor on the first level; (d) the timber joists were firstly positioned and screwed to the lateral beams, then the plywood floor units were inserted and the concrete slab was cast; (e) once the concrete was sufficiently cured, steel masses were bolted onto the concrete slab to simulate the additional masses required by the Prototype versus Test Specimens Cauchy-Froude similitude. For the 3PT pre-stressed timber-concrete floor on the second level; (f) the floor units were positioned on their supporting plates and additional plates/screws (connectors) were introduced to transfer the shear forces to the lateral seismic force-resisting system; (g) the *Skeleton Building* was thus ready to be craned and placed on the shake table; and (h) finally, the driving masses of the second floor were introduced in this final configuration. It is worth noting that the post-tensioning of the strands/tendons of both the seismic beams and the timber-concrete beams

FIGURE 9 Construction/assembly of: (A–C) the fiber-reinforced ceramic gypsum partition; (D–F) the low damage masonry infill wall; (G) the GFRC facades; (H, I) the spider glazing facades.

forming the 3PT floor, as well as the post-tensioning of the threaded bar of the timber walls, were carried out in between the phases (c) and (d) previously described and no re-tensioning was applied once the skeleton building was completed.

5.1 | Construction/installation of the non-structural elements

The construction/installation of partitions and facades for both *Option 1* and *Option 2* configurations was carried out with the specimen on the shake table. After the first testing phase (*Skeleton Building*), the internal fiber-reinforced gypsum partitions were built, and the second testing phase was performed. Then, the internal partitions were demolished and substituted by an infilled low-damage masonry partition in the wall direction. Finally, the exterior enclosures were attached and the third testing phase was carried out. A more comprehensive description of construction details, assembly phases, and non-structural performance can be found in Bianchi et al.[30]

Focusing on the fiber-reinforced gypsum partition walls, the internal steel sub-frame was assembled first (Figure 9A). This frame consisted of vertical studs not screwed to the horizontal guides whilst able to move freely (slide and uplift) inside them. Additional construction details were introduced within the frame, namely: (a) adhesive acoustic sided tape on channels and studs; (b) timber frames to create the door openings, surrounded by lateral steel studs screwed to the top

horizontal guide using a telescopic (slip) joint; and (c) 10 mm of lateral gaps between the horizontal tracks and the concrete columns and between the vertical studs and the upper horizontal channel (Figure 9B). Once the frame was completed, the 25 mm-thick fiber-reinforced ceramic gypsum panels were attached to both sides of the frame. The 600 × 1200 mm boards were properly cut to fit within the available space following an assemblage scheme. These panels were connected together through their tongue-and-groove joints and additional adhesive glue, and screwed to the vertical studs by leaving a 10 mm perimeter gap between the overall wall and the structural system. After the assemblage of the system (Figure 9C), additional glue was applied to the surface to create a homogeneous and smooth wall. The perimeter gap was filled using silicone foam and additional joint cover tape was applied by using adhesive glue. To complete the wall, the perimeter parts were finally covered by silicone sealant.

Concerning the low-damage unreinforced masonry wall, a different steel sub-frame was built on the first floor in the wall direction (Figure 9D). The horizontal steel tracks were fixed to the building floors and the vertical studs inserted within these channels. Internal gaps were introduced in the frame to enable the rocking movement of the independent and adjacent panels: (a) 5 mm gap between the horizontal channels and the concrete columns, between the first steel studs and the horizontal channels and between the internal vertical studs forming the five masonry panels and (b) 10 mm vertical gap between the steel studs and the upper horizontal channel (Figure 9E). Finally, the masonry walls were built inside the steel frame using 90 × 190 × 300 mm bricks and 10 mm mortar (Figure 9F). No mortar was introduced between bricks and steel profiles to allow additional sliding behavior to the rocking walls. The wall was thus completed by filling the horizontal gaps with polyurethane foam. Also, a light white painting was applied to one of the two sides of the wall to help monitoring the possible formation of cracks on the masonry wall during the shake table tests.

The installation of the GFRC facades was simple and fast. The upper steel anchorages (shown in the previous section) were connected to the concrete columns by hammer head bolts inserted within cast-in channels in concrete. Then, the precast concrete panels were lifted and positioned on these sliding hook anchorages (Figure 9G). During this operation, the correct position for the bottom anchorage restraints was checked, and these bottom anchorages (steel assemblies) were appropriately bolted/welded/screwed to the structural skeleton. The restraint anchorages were finally completed by filling the internal part of their rectangular profiles with fast-curing concrete. Regarding the glazed facades, accuracy and precision were required for the assembly of the system. The first construction operation involved the connection of the steel anchorages to the structural system. Specifically, spider connectors were connected through M10 bolts to steel plates properly positioned and fixed to the structural skeleton. After introducing spherical ball joints into the four holes of each glass panel, including 2–3 mm of internal glass/steel tolerance, the glass panels were lifted and connected to the spider/plate system through their 24 mm diameter nuts (Figure 9H). The overall facade was built by assembling three glass panels at the bottom level, then the panels of the upper level were lifted in place and connected (Figure 9I). Internal gaps of 10 mm were left between the glass in both the vertical and horizontal directions and finally filled with sealing tape.

6 | EXPERIMENTAL SET-UP

6.1 | Testing program

The tri-axial shake table of the Laboratório Nacional de Engenharia Civil (LNEC) in Lisbon (PT) has a testing platform of 5.60 m × 4.60 m extensible to 5.60 × 6.20 m, a maximum payload capacity of approximately 400 kN, an excitation frequency range of 0—40 Hz, maximum accelerations of 0.9, 1.6, and 0.6 g in the longitudinal, vertical and transverse directions of the specimen. The maximum displacements in all three axes are equal to ±200 mm. The transverse, vertical, and longitudinal actuators can provide a total maximum force of 750, 1250, and 500 kN, respectively.

As part of the experimental campaign, four levels of earthquake intensity were adopted for the shake table tests, namely: LS1, representing the Operational Limit State (return period (T_R) = 50 years); LS2, representing the Damage Control Limit State (T_R = 100 years); LS3, representing the Life-Safety limit state (T_R = 475 years); LS4 representing a return period of T_R = 1500 years, which is higher than the Collapse Prevention limit state according to the Italian code (where it is set at T_R = 975 years). Three Far Field (EQ_1, EQ_2, EQ_3) and two Near Fault (EQ_4, EQ_5) earthquake records were selected as input motions and scaled to seismic intensity levels (Table 2). All records were taken from the PEER online strong ground motion database. The Far Field records were selected considering a hypocentral depth ranging between 10 and 20 km and a moment magnitude (M_w) greater than 7. The Near Fault records were selected based on the PGV/PGA ratio, at least 0.08 m/s/g and distance from fault (less than 10 km). Records on shallow and deep soils were selected to

TABLE 2 Properties of the selected earthquake motions.

ID	Earthquake	Station	Year	Mw	PGA [g]	Scaling factors			
						LS1	LS2	LS3	LS4
EQ_1	Cape Mendocino	Eureka Myrtle & West	1992	7.0	0.178	0.94	1.35	2.47	3.22
EQ_2	Landers	Morongo Valley	1992	7.3	0.188	0.71	1.02	1.86	2.43
EQ_3	Darfield	REHS	2010	7.1	0.239	0.48	0.69	1.26	1.64
EQ_4	Imperial Valley-06	El Centro Array #4	1979	6.5	0.485	0.35	0.50	0.91	1.19
EQ_5	Christchurch	CCCC	2011	6.3	0.354	0.36	0.51	0.94	1.23
EQ_6	L'Aquila	AQV	2009	7.0	0.496	–	–	–	–

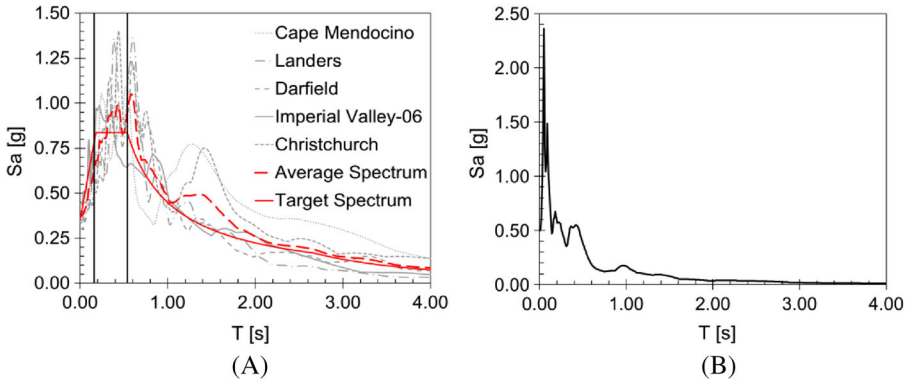

FIGURE 10 Acceleration response spectra of the earthquake records: (A) scaled horizontal components, with average and target spectra at LS3—Life-Safety—and period range for the scaling procedure; (B) unscaled vertical component (EQ_6).

account for different soil amplifications. An additional ground motion (EQ_6), selected from recordings of the 2009 L'Aquila Earthquake, was introduced to provide a high vertical acceleration shaking motion.

The horizontal records (EQ_i, for $i = 1,..5$) were scaled according to the scaling procedure proposed by the NZS 1170.5[38] code with reference to the Life-Safety design spectrum defined according to the Italian Code.[34] Further scaling (in duration, t[s]) was required to take into account the Cauchy-Froude similitude of equal accelerations between the Prototype Building and the Test Building ($t_{Test} = t_{Prototype} \cdot \sqrt{\lambda}$, where $\lambda = 0.5$). Scaling factors were finally introduced to simulate the different seismic intensity levels (LS1-4). Figure 10A shows the scaled acceleration response spectra and the average spectrum of the horizontal ground motions at the Life-Safety limit state, while Figure 10B shows the response spectrum for EQ_6, representing the vertical component (2009 L'Aquila earthquake) to be applied in combination with the horizontal input motions to create triaxial signals. The selected vertical signal was not scaled with the intention of simulating a real earthquake characterized by a high vertical intensity shaking.

The experimental campaign was carried out by incrementally increasing the seismic intensity in different directions, namely: the longitudinal (X) or frame direction, the transverse (Y) or wall direction, a 45° diagonal direction in the horizontal plane (XY) and the vertical direction (Z). The test sequence involved: (1) 1D input motions in both the longitudinal (EQi—X or EQi—Y) and vertical (EQ6—Z) directions; (2) 2D correlated input motions (EQi—XY), by applying X and Y record components to simulate the earthquake at a 45° angle of attack; and (3) 3D input motions by combining the XY input with the vertical excitation (EQi—XY + EQ6—Z), the latter having its peak values a few seconds before the peak response to the XY earthquake. In addition to the ground motion sequence, "white noise" signals (maximum amplitudes of 2–6 mm, duration of 165 s, and maximum frequency of 40 Hz) were run before and after each intensity level to induce low-magnitude vibrations of the specimen that were used for system dynamic identification. The natural frequencies of the specimen in both building directions were identified by means of Frequency Response Function estimations.[39] Table 3 shows the testing sequence followed for each testing phase (*Skeleton Building*, *Option 1*, *Option 2*). All the earthquakes $EQ_{1\text{-}6}$ (or selected, in case of higher intensities and for *Option 1–2*) were tested at the different limit states (LS1-4), meaning that the LSi X, LSi Y, LSi XY sequence (in Table 3) was repeated for each EQ_i before performing the white noise signal. It is however highlighted that not all the 5 EQi were considered at each limit state level. As a result, the experimental campaign involved a total number of 146 input ground motion tests and 42 white noise tests.

TABLE 3 Testing sequence of each testing phase.

Record ID	Input motion description
00_Z, 00_X, 00_Y	Pre-seismic, White noise signal in Z, X, and Y directions
LS1_EQ$_i$_X	LS1, EQ$_i$, X direction
LS1_EQ$_i$_Y	LS1, EQ$_i$, Y direction
LS1_EQ$_i$_XY (45°)	LS1, EQ$_i$, XY (45°) direction
01_X, 01_Y	Post-LS1, White noise signal in X and Y directions
LS2_EQ$_i$_X	LS2, EQ$_i$, X direction
LS2_EQ$_i$_Y	LS2, EQ$_i$, Y direction
LS2_EQ$_i$_XY (45°)	LS2, EQ$_i$, XY (45°) direction
02_X, 02_Y	Post-LS2, White noise signal in X and Y directions
LS3_EQ$_i$_X	LS3, EQ$_i$, X direction
LS3_EQ$_i$_Y	LS3, EQ$_i$, Y direction
LS3_EQ$_i$_XY (45°)	LS3, EQ$_i$, XY (45°) direction
03_X, 03_Y	Post-LS3, White noise signal in X and Y directions
EQ$_6$_Z	EQ$_6$, Z direction
LS4_EQ$_i$_XY (45°) + EQ$_6$_Z	LS4, EQ$_i$, XY (45°) Direction + EQ$_6$, Z direction
04_X, 04_Y	Post-LS4, White noise signal in X and Y directions

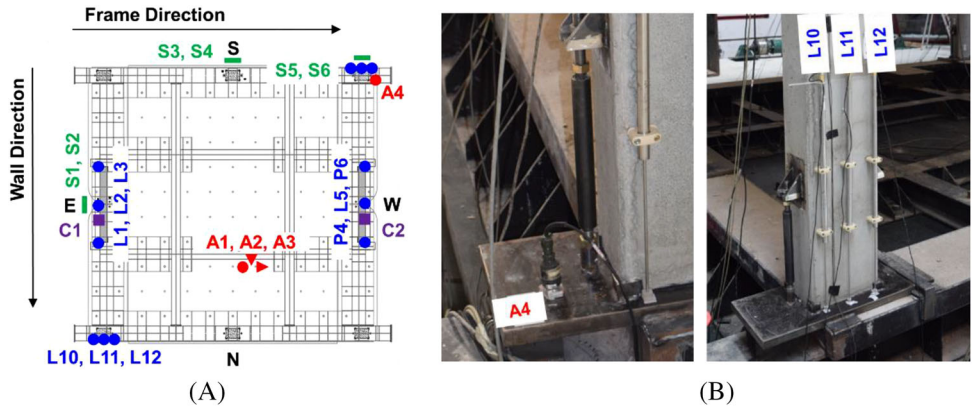

FIGURE 11 Instrumentation layout for the foundation level: (A) accelerometers (A), LVDTs (L), potentiometers (P), strain gauges (S); (B) accelerometer and LVDT transducers at the column base in the South-West corner.

6.2 | Instrumentation plan

The monitoring system of the specimen consisted of a combination of sensors, for a total number of 78 instrumentation channels, including accelerometers (ENDEVCO 7290-A and PCB Piezotronics 337A26), LVDT transducers (RDP Electronics ACT2000C, ACT4000C, ACT6000), optical devices (HAMAMATSU C5949), load cells (maximum capacity of 200 kN) and strain gauges (HBM 1-LY11-6/120, 1-LY11-10/120). The instrumentation was used to monitor: (a) the global behavior of the building system; (b) the local response of the hybrid connections; and (c) the in-plane/out-of-plane seismic performance of the non-structural elements. The monitoring system was designed to record as much information as possible, considering the high number of components involved during the experimental program and the limitations in terms of maximum channels for data acquisition.

During the first testing phase, all sensors were used to monitor the seismic response of the main structure and its connections. At the foundation level (Figure 11A): (1) accelerometers were used to record the input accelerations of the shake table in the three directions (A1, A2, A3) and to study the impact effect at the base of a rocking column (A4, Figure 11B) and (2) LVDT transducers or potentiometers, positioned at the center and at both edges of the base of the structural members (Figure 11B), monitored the opening/closing of the gap at the base of two opposite

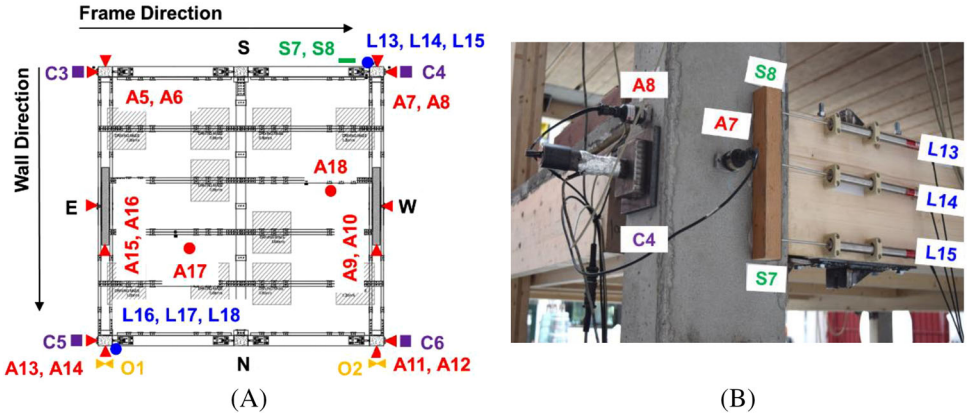

FIGURE 12 Instrumentation layout for the first building level: (A) accelerometers (A), LVDTs (L), strain gauges (S), optical devices (O); (B) photo of the sensors located in the South-West beam-column joint.

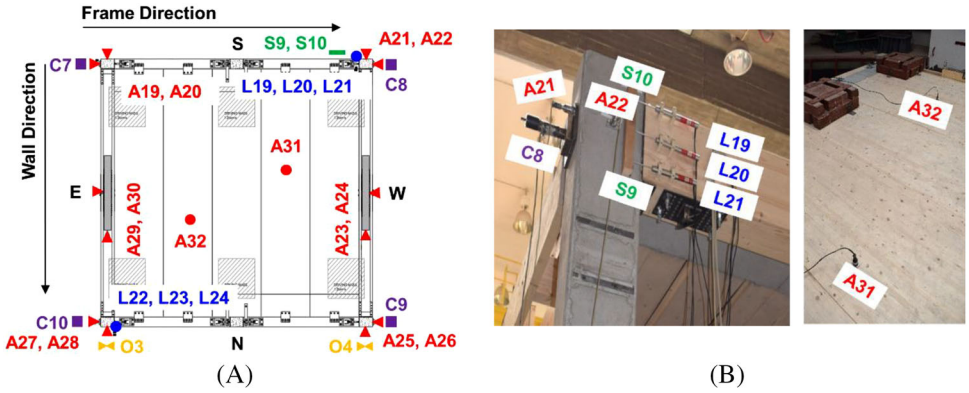

FIGURE 13 Instrumentation layout for the second building level: (A) accelerometers (A), LVDTs (L), strain gauges (S), optical devices (O); photos of (B) sensors located in the South-West beam-column joint; and (C) accelerometers on the 3PT floor.

(N-E and S-W corners) rocking concrete columns and of the timber walls. At the floor level, accelerometers (in both X and Y directions) were introduced to monitor the four lateral columns in the specimen corners, the two timber walls in both the in-plane and out-of-plane directions and the vertical accelerations on the timber-concrete floors (A17, A18, A31, A32). Also, LVDT transducers monitored the opening and closing of the gaps at the beam-column interface for two opposite corners (N-E, S-W). Figures 12 and 13 schematically show the instrumentation layout designed for both building floors in the first testing phase (*Skeleton Building*). Furthermore, 2D optical devices recorded the displacements of the structural frame in the North side, while load cells acquired the variation of the post-tensioning force in the seven wire strands/tendons (beams) and in the threaded bars (walls) during the earthquake shakings. These load cells (C1, C2, Figure 11) were connected to the tendons/bars before the initial post-tensioning carried out during the construction sequence. Finally, strain gauges were attached to some of the external dissipaters (at the column/wall-foundation base, at the beam-column joint) in order to record the strain and thus, indirectly, the stress and force developing under the seismic motions. These strain gauges were fixed on the internal fuse of the *Plug&Play* dissipaters by applying a specific glue, then the dissipaters were completed by filling their steel tubes with epoxy for anti-buckling purposes. Before bolting the *Plug&Play* into their anchorages, the monitored dissipaters were subjected to tension testing until the elastic range with the aim of calibrating the strain gauges.

Due to the need for monitoring both the main structure and the internal partitions during the second testing phase (*Option 1*), some of the accelerometers and transducers were removed from the structural system and positioned on the internal fiber-gypsum partitions. The partition walls were monitored as shown in Figure 14. Specifically, five accelerometers were distributed on the wall surface to record the out-of-plane response, while four LVDT transducers were installed to monitor the in-plane movements/deformations in the orthogonal directions. The behavior of the partition in the

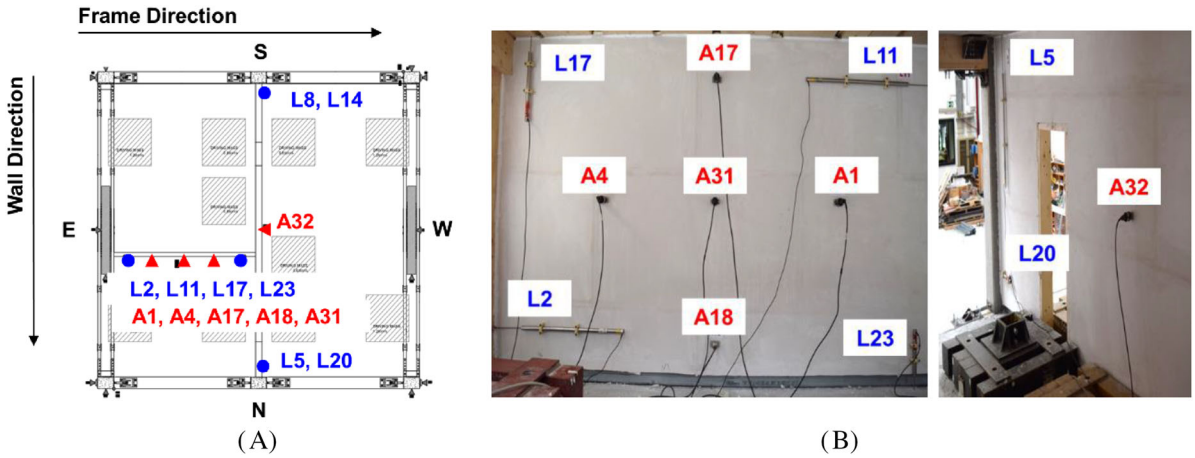

FIGURE 14 Monitoring system for the fiber-reinforced gypsum partitions: (A) general layout and (B) photos.

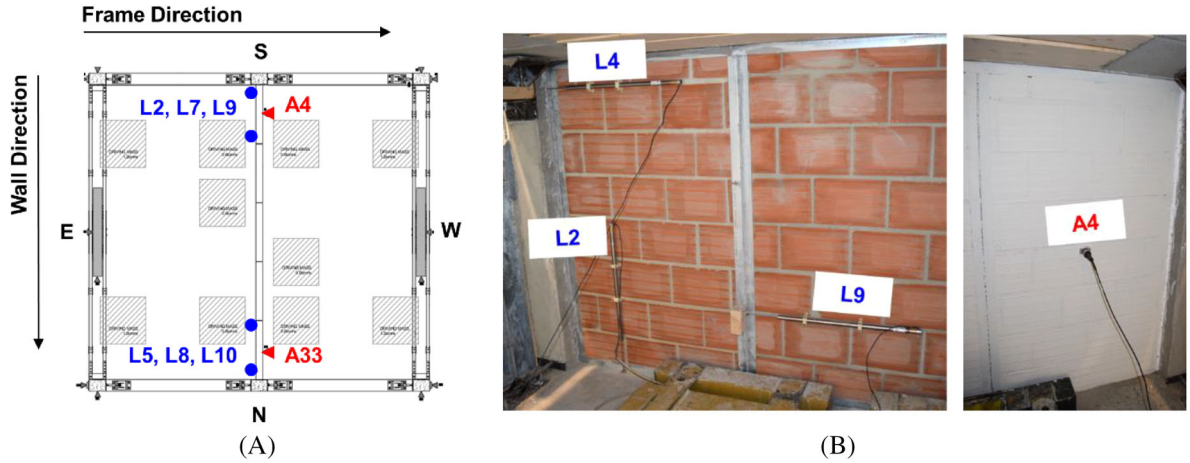

FIGURE 15 Monitoring system for the low-damage masonry partitions: (A) general layout and (B) photos.

transverse direction was studied through one accelerometer located at the mid-height of the panel (at the intersection between the two orthogonal walls) and four displacement transducers in the in-plane direction.

Focusing on the last specimen configuration (*Option 2*), a new instrumentation plan was designed due to the high number of components involved. Regarding the masonry partition, the two lateral rocking walls were only monitored by using: (1) LVDTs to measure the horizontal displacements relative to the column and between two adjacent walls, and the vertical wall/floor relative displacements and (2) an accelerometer was positioned at the center of the wall to record the out-of-plane accelerations (Figure 15). The cladding facade in the North side was monitored as shown in Figure 16A. More specifically, accelerometers were installed to control both the in-plane and the out-of-plane accelerations, while LVDTs monitored the cladding-column relative displacements, as well as the relative displacements between adjacent panels. For the GFRC facade in the South side, only the structural/non-structural relative displacement was recorded. The glass facade in the East side was monitored as presented in Figure 16B, namely using (1) accelerometers to record the in-plane accelerations at the spider connectors and at the middle height of the panel, and the out-of-plane accelerations at the center of the panel and along the diagonal and (2) LVDTs to monitor the relative displacements in the horizontal and vertical directions between the facade and the main structure as well as between adjacent panels. The glass facade in the West side was instead monitored in terms of relative structural/non-structural displacements.

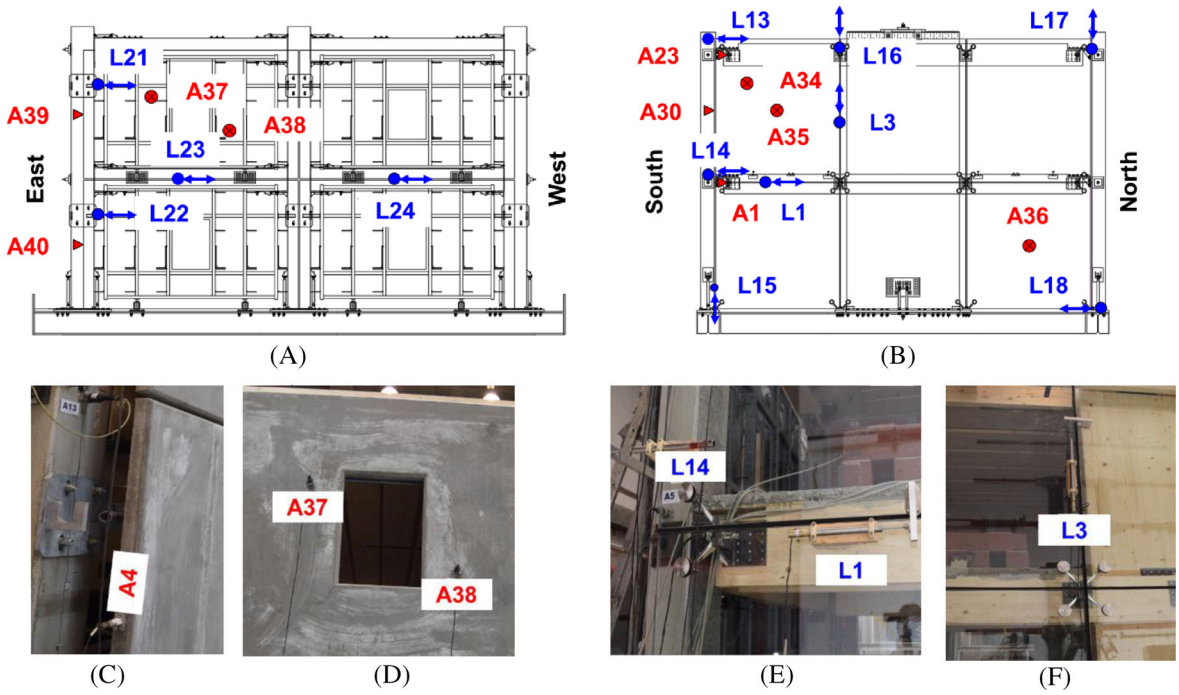

FIGURE 16 Instrumentation layout for: (A) the Glass Fiber Reinforced Concrete facade in the North side; (B) the Spider Glazing facade in the East side; (C–F) photos of some sensors.

7 | EXPERIMENTAL RESULTS

7.1 | Signal post-processing

The LNEC shake table is controlled by compatible displacement and acceleration time series sampled at 200 Hz. The digital signal processing of the results in both time and frequency domains, including decimation, filtering, integration, differentiation, and detrending, was carried out using the LNEC-SPA software.[39] The recording of data was carried out through a high-speed data acquisition system. All data was collected at a sample frequency of 4000 Hz to avoid spurious aliasing effects and decimated at 200 Hz. A Fourier low-pass filter at 35 Hz was applied to all recorded data. Additionally, a Butterworth bandpass filter was applied to the acceleration data across the frequencies of 0.1–20 Hz to eliminate noise outside of the range of building excitation and response.

7.2 | Seismic demand

Inter-storey drift ratios (e.g., Figure 17—*Option 1*, EQ_2 at LS_3) and floor accelerations were measured for each shaking direction, building level, and input motion at increasing seismic intensities. The maximum values of these engineering demand parameters (e.g., Figure 18—*Option 1*) were calculated for all the test phases and are summarized in Table 4, while Figure 19 presents the maximum quantities recorded during the full experimental campaign. The peak accelerations (out-of-plane and/or in-plane) on the non-structural elements and their maximum displacements relative to the primary structure are also included in the same table. It can be noticed that inter-storey drift ratios and floor accelerations are mostly reduced when moving from the *Skeleton Building* to the integrated systems. This was mainly due to the testing sequence, involving all the input motions in mono-directional (1D) shakings for the *Skeleton Building* until LS3 (EQ_2 at LS3 was only performed as 1D input for *Option 1*), while a combination of horizontal shakings (2D) at the maximum intensity levels (LS3-4) was performed for the other specimen configurations (*Option1*, as noticed in the testing sequence highlighted in Figure 18, and *Option2*). When comparing the results for the same intensity level (Table 4), it can be observed that (1) the gypsum walls did not influence the seismic global response in *Option 1* (the difference between *Skeleton* and *Option 1* response observed in the wall direction was due to an increase of the post-tensioning force in the timber walls carried out

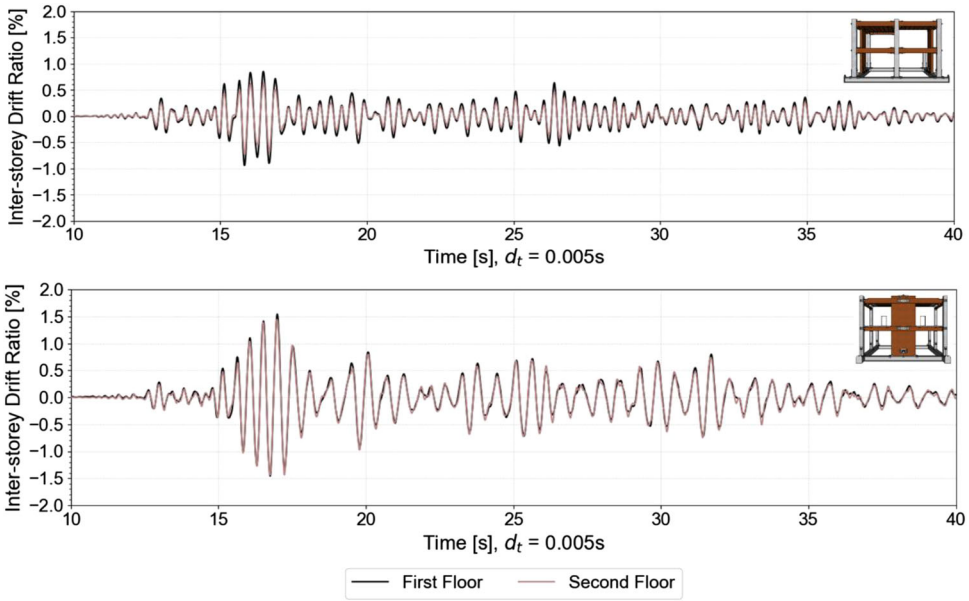

FIGURE 17 Inter-storey drift ratios recorded for *Option 1*, for example, EQ_2 at LS3 (EQ_2_X and EQ_2_Y input for frame and wall directions, respectively).

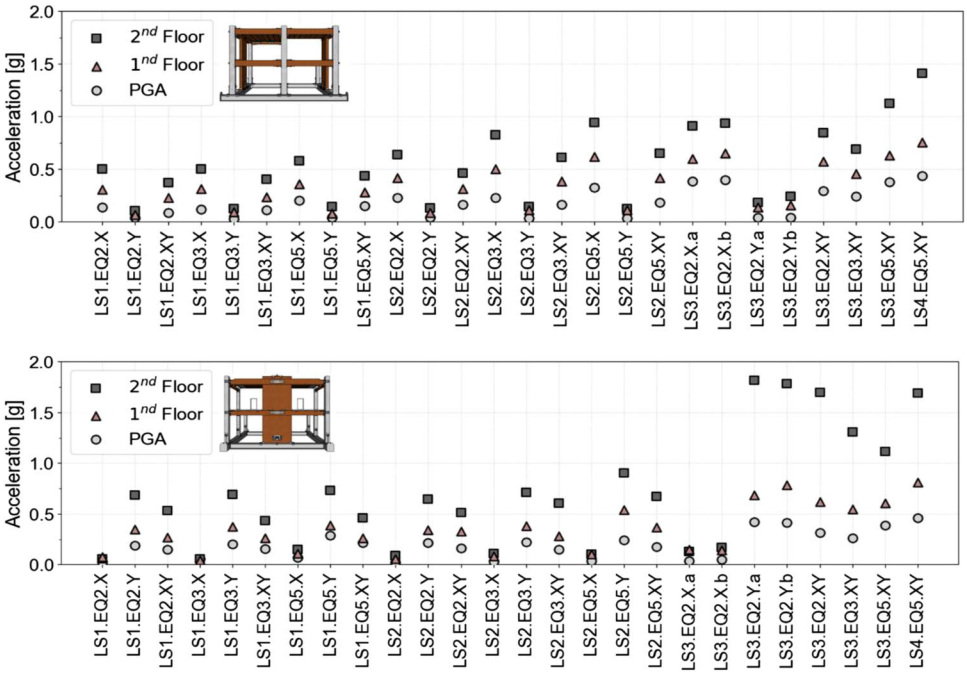

FIGURE 18 Peak Ground Accelerations (PGA) and maximum floor accelerations recorded during the full testing sequence for *Option 1*.

before the tests on *Option 1*; this was needed in order to adjust the self-centering ratio at the wall base connection before starting the experiments on *Option 1*) and (2) when comparing *Option 1* and *Option 2*, the influence of non-structural elements (leading to a reduction of drift and acceleration values) can mainly be noticed in the wall direction, where more components were installed.

A comparison of seismic demand for *Option 1* versus *Option 2* is shown in Figures 20 and 21, where all the drift/acceleration results (and mean values) are summarized for all the intensities. Although a direct comparison could be made at the low earthquake levels which involved the same testing sequence (only one triaxial input was performed at

TABLE 4 Summary of the maximum recorded structural and non-structural response parameters.

Intensity level		LS1		LS2		LS3		LS4	
Direction		**Frame**	**Wall**	**Frame**	**Wall**	**Frame**	**Wall**	**Frame**	**Wall**
Skeleton Building									
Acceleration [g]	Table	0.17	0.21	0.47	0.27	0.32	0.34	–	–
	Floor 1	0.36	0.35	0.50	0.57	0.65	0.74	–	–
	Floor 2	0.58	0.62	0.76	1.38	0.99	1.89	–	–
Inter-storey drift ratio [%]	Level 0/1	0.61	0.49		1.20	1.21	1.79	–	–
	Level 1/2	0.42	0.51		1.26	1.02	2.00	–	–
Option 1									
Acceleration [g]	Table	0.17	0.20	0.29	0.25	0.35	0.38	0.35	0.43
	Floor 1	0.36	0.39	0.59	0.54	0.65	0.78	0.71	0.81
	Floor 2	0.58	0.73	0.92	0.90	1.10	1.82	1.37	1.69
	Partition	0.53	1.20	0.86	1.27	0.99	1.64	1.12	1.68
Inter-storey drift ratio [%]	Level 0/1	0.53	0.51		0.62	1.02	1.64	1.22	1.32
	Level 1/2	0.41	0.43		0.60	0.87	1.56	1.19	1.31
Relative displ. [mm]	Partition	5.49	1.23	12.82	1.67	14.01	9.72	12.75	6.48
Option 2									
Acceleration [g]	Table	0.14	0.17	0.22	0.17	0.34	0.32	0.41	0.47
	Floor 1	0.28	0.33	0.44	0.35	0.58	0.57	0.68	0.67
	Floor 2	0.45	0.62	0.63	0.56	1.02	1.05	1.21	1.41
	GFRC fac.	–	0.79	–	0.79	–	1.12	–	1.52
	Spider fac.	0.59	0.39	0.97	0.35	1.09	0.69	1.47	0.99
	Partition	0.40	–	0.55	–	0.82	–	0.96	–
Inter-storey drift ratio [%]	Level 0/1	0.39	0.33	0.60	0.36	0.90	0.80	1.24	0.98
	Level 1/2	0.33	0.37	0.79	0.34	0.67	0.74	0.84	1.04
Relative displ. [mm]	GFRC fac.	3.97	–	5.52	–	9.21	–	12.15	–
	Spider fac.	–	2.76	–	2.38	–	4.55	–	5.32
	Partition	–	3.02	–	1.93	–	6.53	–	9.91

LS4 for *Option 1*, while only triaxial motions were performed at LS3-4 for *Option 2*), it is found that: (i) higher drift ratios were recorded for the first inter-storey in the frame direction (as observed in Table 4), due to the predominant first mode affecting the response, while first inter-storey drift ratios are comparable to the second inter-storey drift ratios for the wall direction, as a result of the linear deformed shape of the wall; (ii) the floor accelerations doubled when moving from the first-storey to the second one, (iii) the frame and wall systems behaved similarly at low seismic intensities (LS1-2) while higher seismic demand was observed in the wall direction for higher seismic intensities (LS3-4), due to the concentration of inelastic deformations at one connection only (wall-foundation), (iv) reduced drift and acceleration values were found for *Option 2* as a consequence of the higher influence of non-structural components due to the overall higher stiffness and to the damping of the façade/structure connections.[30]

Overall, the specimens behaved very well as expected, with seismic demand parameters consistent with the design approach and modeling predictions. This is discussed in detail in Ciurlanti et al.,[29] where the comparison of analytical versus numerical versus experimental results for the primary structure confirms a very satisfactory accuracy of the numerical modeling based on a lumped-plasticity approach[40] developed to predict the response of these rocking-dissipative systems. Regarding the non-structural elements, the in-plane behavior demonstrated the efficiency of the adopted construction details, while the out-of-plane accelerations allowed to identify amplification factors relative to the first building floor acceleration in the range of 2–3. As mentioned above, a better investigation on the seismic demand/performance for all the partitions and facades can be found in Bianchi et al.[30]

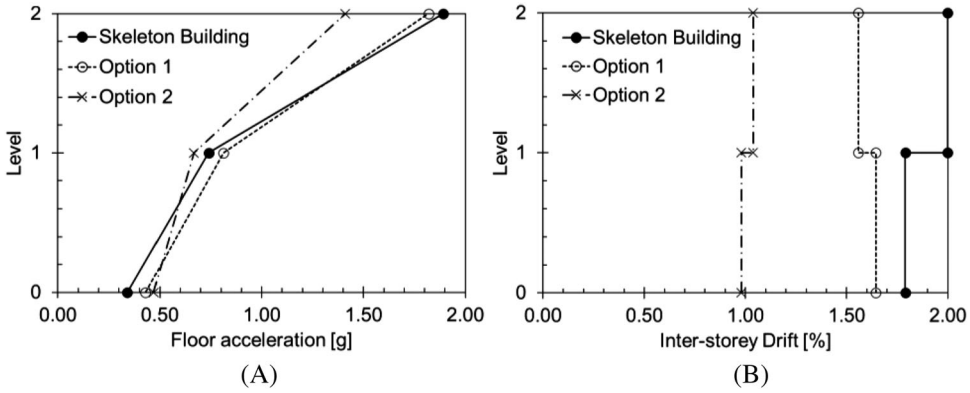

FIGURE 19 Peak floor accelerations and maximum inter-storey drift ratios recorded during the tests (maximum of both structural directions) for all specimen configurations.

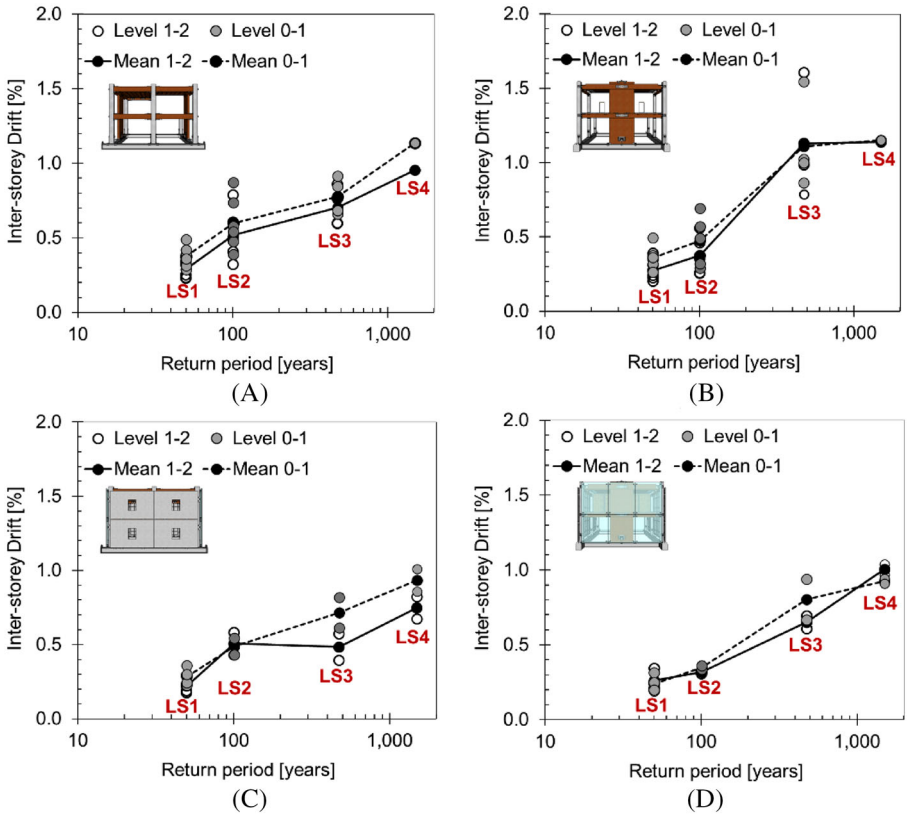

FIGURE 20 Maximum inter-storey drift ratios (and average values) recorded during the tests for: *Option 1*—(A) frame and (B) wall direction; *Option 2*—(C) frame and (D) wall direction.

7.3 | Dynamic identification

The dynamic response of the specimens was investigated in terms of modal frequencies and, consequently, damage assessment. As indicated above, dynamic identification of the Test Building was carried out after each intensity level sequence by applying low-intensity white noise signals. Table 5 lists the frequencies of the first mode of vibration for *Option 1* and *Option 2* (*Skeleton Building* is not comparable in the wall direction due to the change in the post-tensioning of the wall, as discussed in the previous section). A modal testing by impact hammer was performed before/after the seismic tests to study the dynamic behavior of specific partition walls and facade panels: (1) the gypsum partition in the frame direction; (2) the upper-left GFRC panel of the North side facade; (3) the upper-left panel of the East side glazing wall; and (4) the

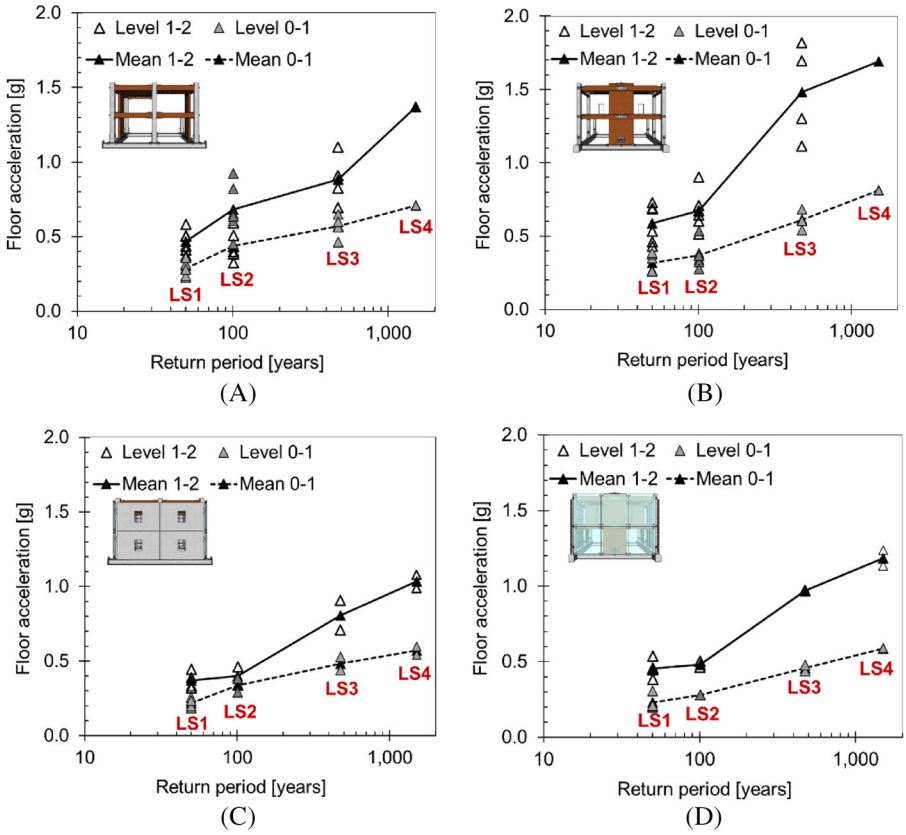

FIGURE 21 Peak floor accelerations (and average values) recorded during the tests for: *Option 1*—(A) frame and (B) wall direction; *Option 2*—(C) frame and (D) wall direction.

TABLE 5 Frequencies [Hz] of the first mode of vibration of the building and of the partitions/facades.

Configuration	Option 1			Option 2				
System	Frame direction	Wall direction	Gypsum wall	Frame direction	Wall direction	GFRC panel	Glass panel	Masonry wall
Initial	3.50	3.71	21.00	3.66	3.90	16.27	69.00	37.35
After LS1	3.37	3.12	20.00	3.53	3.87	16.02	69.00	37.05
After LS2	3.08	3.12	19.71	3.47	3.71	–	–	32.44
After LS3	3.03	2.59	19.06	3.35	3.32	15.43	68.75	26.17
After LS4	2.88	2.54	18.70	3.08	2.98	15.27	68.59	15.02

masonry partition in the North corner. The natural frequencies of these components could be identified by applying the transfer function method and are shown in the same Table 5.

Although a direct comparison between the frequency/period of the structure with (*Option 1*) or without (*Skeleton Building*) gypsum partitions cannot be made in the wall (Y) direction (due to the modification in the post-tensioning of the wall between the two testing phases), the gypsum partitions had negligible impact in the overall building response as a consequence of its reduced additional mass when compared to the mass of the structure as well as of the non-structural construction details designed to reduce the structural/non-structural interaction. As shown in Table 4, the similar seismic demand obtained in the frame direction (X) for both specimen configurations (*Skeleton Building* and *Option 1*) confirms this. Comparing the first natural period for both building directions for *Option 2* versus *Option 1*, it is found that the stiffness provided by the masonry wall and facades, although partly decoupled from the main structure in terms of displacement compatibility, reduced the building periods in both directions.

When comparing the different testing phases (LS1-4), a reduction of frequency can be noticed in both structural directions. For the main structure, this was mostly due to the yielding and consequent permanent deformations of the external

TABLE 6 Damage observed during the experiments.

Intensity level	Max. inter-storey drift ratio [%]	Max. floor acceleration [g]	Structural damage	Non-structural damage
LS1	0.43	0.73	–	Gypsum partitions: 0.04 mm diagonal cracks at the corners of the opening
LS2	0.60	0.90	–	Gypsum partitions: 0.1–0.3 mm diagonal cracks at the corners of the door; detachment of the silicone sealant and loss of adhesive in the cornersMasonry partition: initial detachment of silicone sealant in the corners, initial sliding of the walls inside the frames
LS3	1.56	1.82	Yielding of *Plug&Play* dissipaters	Gypsum partitions: 0.15–0.65 mm diagonal cracks at the corners of the door of the gypsum partition
LS4[a]	1.32	1.69	Torsion of seismic beams due to pounding of the 3PT timber-concrete beams	Gypsum partitions: >2 mm diagonal cracks at the corners of the door of the gypsum partition; initial crushing of the panels in some cornersSpider glazing: yielding of the ball joints in the out-of-plane directionMasonry partitions: cracking of the mortar surrounding one brick

[a]LS4 involved bi-directional motions only, thus the max. recorded values were less than LS3.

dissipaters, especially those located at the wall base. Nevertheless, this loss of capacity was mainly caused by the high number of shaking tests to which these elements were subjected during the experimental campaign. Although no collapse of the dissipaters was observed, they were nevertheless completely substituted between each test configuration, that is, *Skeleton Building*, *Option 1*, and *Option 2*, to avoid possible effects of accumulated damage on the comparison of the results. On the other hand, the slight-to-moderate reduction of frequencies for the non-structural systems highlighted loss of stiffness and potential loss of capacity. Specifically, Table 5 shows: (1) no reduction of frequencies for the glass panels, meaning a completely undamaged component after testing, (2) very limited reductions for the fiber-gypsum partition as well as the GFRC facade, while (3) for the infill partition wall a modification of the natural vibration was mainly noticed when moving from LS2 (Serviceability) to the LS3 (Life-Safety). This shift of frequency was due to the controlled rocking movement of the masonry walls inside the steel frame during the shaking, producing an increased clearance/disconnection at the boundaries and consequent loss of stiffness.[30]

7.4 | Damage observation

Overall, very low damage to both main structure and partitions/facades was found, confirming the high potential and benefits of implementing earthquake-resistant solutions. The fact that a small amount of damage was observed, as discussed below and summarized in Table 6, shows that the ambition of a "no-damage" seismic design concept is not yet fully realized, but certainly, the response can be described as "low-damage."

It is worth noting that the extensive experimental campaign, comprising more than 150 excitations, clearly represented a particularly severe and demanding sequence of simulated earthquake events, which would be unrealistic even within a typically assumed 50- or 100-years design life of a building. More specifically, yielding and associated permanent deformation/elongation of the *Plug&Play* external replaceable dissipaters were observed as part of the expected damage conditions for rocking-dissipative systems with external dissipaters (Figure 22A). This damage state was achieved after many shakings and particularly beyond the Life-Safety test sequence (LS3). During the controlled rocking/dissipative mechanism, the inelastic demand was indeed accommodated within these sacrificial fuses which—if needed—could easily be replaced after an earthquake event with a low cost. No other damage was found to the structural beams, columns, and walls. The expected design maximum strain of the devices at LS3 was expected to be 3.5%.

Another source of structural damage—more related to the testing apparatus—was observed in the central beam of the TCC floor. Due to the presence of six steel masses (around 3.6 tons) on the influence area of these beams, these masses did

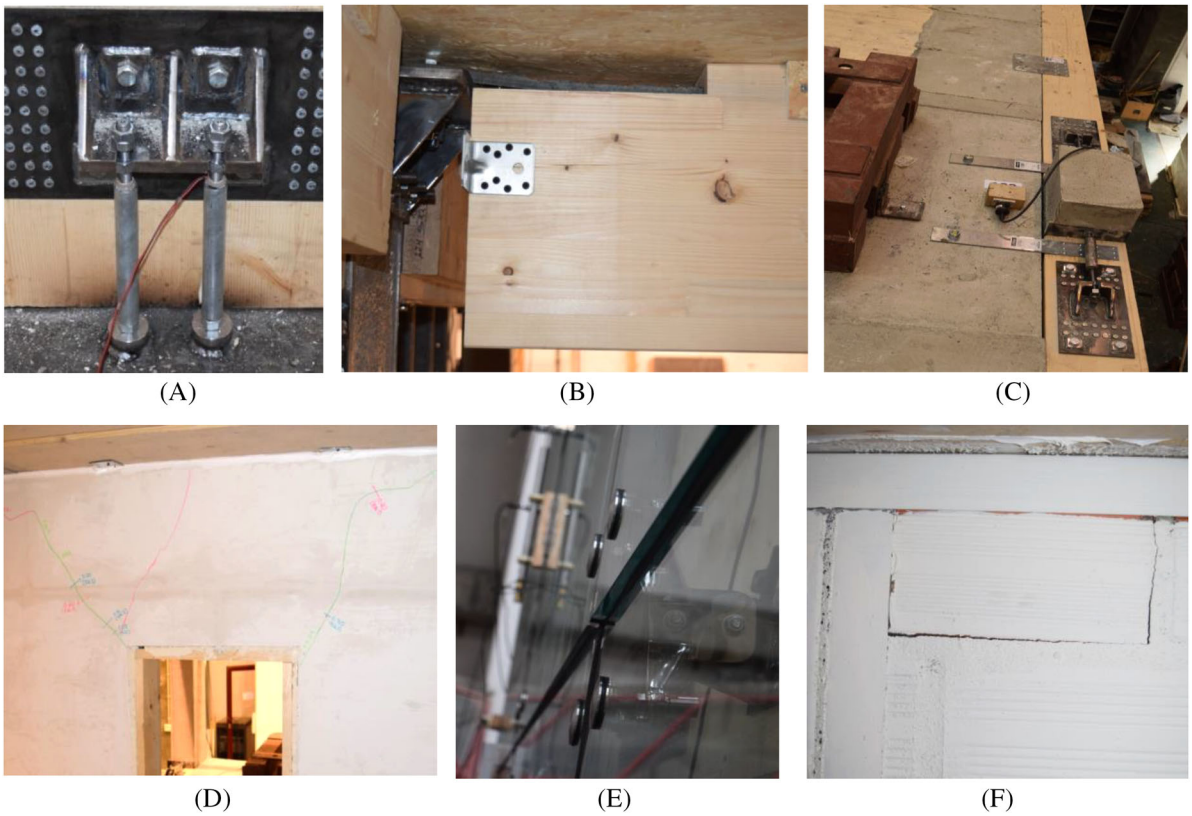

FIGURE 22 Structural and non-structural damage: (A) yielding of the external dissipaters; (B) damage to the end sections of the central gravity beam due to vertical loading; (C) pounding effect of the 3PT beams; (D) diagonal cracking of the gypsum partitions; (E) out-of-plane displacements of the glass panels; (F) cracking of mortar surrounding a brick of the infill wall.

not only contribute to the horizontal seismic mass but also provided additional vertical accelerations to the building floor which led to very high vertical forces, bending and torsional moments acting on the central timber beams. Therefore, initial cracking to the end sections, bending of the lateral plates and initial withdrawal of some coach screws were observed at the end of the experimental campaign (Figure 22B). Finally, another damage condition for the main structure was observed at the 3PT flooring system (Figure 22C). During the tests, the timber-concrete beams pounded against the supporting lateral seismic beams leading to some rotation (torsion) around their axis. This issue was due to both the forces/moments provided by the driving masses on the second floor and to an inadequate detailing of the test-building configuration, that is, excessively heavy steel supports for the timber-concrete beams as well as the need for more plates on the top of the slab to allow for a better transfer of shear force to the structural lateral frames.

Damage to the non-structural elements was observed. even if at a significantly lower level and for significantly higher demand when compared to traditional solutions used in current construction practice.[21] During the seismic tests, damage to the fiber reinforced gypsum partition was mainly due to the diagonal cracking at the corners of the door openings (Figure 22D). These cracks formed during the LS1 intensity test sequence (less than 0.04 mm crack width at inter-storey drift ratios of around 0.4%) and continued to open until the end of the tests (0.10–0.30 mm at LS2, 0.15–0.65 mm at LS3, greater than 2 mm in some parts after LS4). Detachment of the silicone sealant and loss of adhesive in the corners of the partition wall was observed from LS2, while after LS4 crushing of the panels was noticed in some corners of the wall. The GFRC facade components exhibited a very high seismic performance during the earthquake shaking and no damage was observed after the entire testing sequence. No cracking of the glass panels in the spider glazing system was observed and they behaved very well in the in-plane direction. However, significant residual displacements in the out-of-plane direction of the glass panels relative to each other (maximum values around 14 mm) were recorded (Figure 22E). This was due to the yielding and elongation of the ball joints (around 5 mm) subjected to high forces due to the inertia forces provided by the glass wall in the transverse direction. Lastly, the seismic behavior of the unreinforced masonry wall confirmed the high potential of applying low-damage details to such type of heavy partition/infill wall. Overall, the infill wall did not suffer any significant in-plane damage and did not lose its out-of-plane capacity. No dam-

age was observed after the first two levels of seismic intensity, then initial detachment of silicone sealant in the corners as well as initial sliding of the masonry walls inside the frames were noticed. After the last seismic intensity sequence, LS4, cracking of the mortar surrounding one brick located in the upper-left corner of a rocking wall was also observed (Figure 22F).

8 | CONCLUSIONS

A triaxial shake table experimental campaign was carried out at the Laboratório Nacional de Engenharia Civil in Lisbon, Portugal, as part of the EU-funded project, titled "*(Towards the) Ultimate earthquake proof building system: development and testing of integrated low-damage technologies for structural and non-structural elements*." Shake table tests were performed on a 1:2 scale two-storey timber-concrete building system consisting of low-damage frame and wall structural systems. Different scenarios were investigated; structural skeleton only (*Skeleton Building*), structural skeleton plus lightweight fiber-reinforced gypsum partitions (*Option 1*), and the fully integrated building with partitions and facades (masonry partitions, spider glazing, and glass-fiber reinforced concrete facades, *Option 2*).

The paper described the research project from the design of the scaled building and its structural and non-structural details, to the construction/assembly phases, the test set-up and the experimental results in terms of seismic demand, that is, floor accelerations (up to 1.89 g), inter-storey drift ratio (up to 2%), and seismic performance, through damage assessment and dynamic identification. The latter highlighted a reduction of frequencies in the main structure under increasing levels of seismic excitation, which was mostly due to the yielding plastic deformations (not failure) of the external *Plug&Play* dissipaters in the dissipative post-tensioned rocking connections. Since the dissipaters are the only sacrificial elements of the technology, it is worth mentioning that they have been conceived to be manufactured in a cost-effective fashion and be replaced very easily such that there is no impact to the overall cost of the construction of the system and post-earthquake repairability. On the other hand, a slight-to-moderate reduction of frequencies was observed for the non-structural systems, which translates to loss of stiffness as confirmed by the damage observation. However, the initiation of (slight) damage for the tested non-structural elements was observed for significantly higher displacement demand (LS3, LS4) when compared to current construction practice solutions. More importantly, when testing and comparing the different specimen configurations, it appeared evident that the non-structural elements, although designed with low-damage features, that is, minimal interaction with the structural lateral load system, plaid a role in the reduction of the overall displacements demands of the whole integrated system (*Option 2*).

The experimental program showed an excellent seismic performance of the overall integrated low-damage building system, confirming its unique potential and opportunity for widespread implementation in design and construction practice. Yet, the observed (albeit) slight damage conditions, in particular to the flooring systems and its connection with the structural skeleton, suggest further improvements to the system detailing to be applied in future applications.

ACKNOWLEDGMENTS

The experimental project described in this paper has received funding from the European Union's Horizon 2020 research and innovation programme under grant agreement No 730900. The project offered access to the experimental facilities of the Laboratório Nacional de Engenharia Civil in Lisbon (PT) and supported financially the construction of the Test Building and its various configurations. The authors are grateful to all the partner companies involved in the project, for providing the material and for their practical advice during the preparation of the specimen, namely: LA Cost Srl for the timber and steel components as well as for the coordination of the pre-assembling and shipping; Generale Prefabbricati SpA for the GFRC facades and concrete columns; Glass Point Studio Srl and Cristal Vetri Srl for the glass facades; Gessi Roccastrada Srl for the fibre-reinforced gypsum walls; Jamosil Lda for the masonry infill walls and for the construction of the Test Building configurations.

DATA AVAILABILITY STATEMENT

The data that support the findings of this study are available from the corresponding author upon reasonable request.

REFERENCES

1. Pampanin S. Reality-check and Renewed challenges in Earthquake Engineering: implementing low-damage structural Systems – from theory to practice. *Bull N Z Soc Earthq Eng*. 2012;45(4):137-160. December, ISSN 1174–9875, Keynote Lecture at the 12th World Conference on Earthquake Engineering, Lisbon.

2. Pampanin S. Towards the "ultimate earthquake-proof" building: development of an integrated low-damage system. In: Ansal A, ed. *Chapter in Perspectives on European Earthquake Engineering and Seismology*. 2015:321-358. Series: Geotechnical, Geological and Earthquake Engineering Vol. 39, Chapter 13.
3. SEAOC (Structural Engineers Association of California). *Performance-Based Seismic Engineering*. SEAOC Vision 2000. SEAOC; 1995.
4. EERI (Earthquake Engineering Research Institute). *Functional Recovery: A Conceptual Framework with Policy Options*. EERI; 2019.
5. Johnston HC, Watson CP, Pampanin S, Palermo A, Shake table testing of an integrated low-damage frame building. In Proc., NZSEE Conference, Auckland, New Zealand; 2014.
6. Pampanin S. (Towards the) Ultimate Earthquake proof Building System: Development and Testing Of Integrated Low-Damage Technologies for Structural and Non-Structural Elements. SERA Project, Research Project Proposal, 2017. https://sera-ta.eucentre.it/sera-ta-project-06/
7. Cornell CA, Jalayer F, Hamburger RO, Foutch DA. Probabilistic basis for 2000 SAC Federal Emergency Management Agency steel moment frame guidelines. *J Struct Eng*. 2002;128(4):526-533.
8. Porter KA, An overview of PEER's performance based earthquake engineering methodology. In Proc., 9th International Conference on Applications of Probability and Statistics in Engineering, San Francisco, CA; 2003.
9. Bruneau M, Chang SE, Eguchi RT, et al. A framework to quantitatively assess and enhance the seismic resilience of communities. *Earthquake Spectra*. 2003;19(4):733-752.
10. Sheffi Y, Rice JB. *A Supply Chain View of the Resilient Enterprise*. MIT Sloan Management Review; 2005.
11. Henry RS, Zhou Y, Lu Y, et al. Shake-table test of a two-storey low-damage concrete wall building. *Earthq Eng Struct Dyn*. 2021;50:3160-3183. doi:10.1002/eqe.3504
12. Newcombe MP, Pampanin S, Buchanan AH, Experimental testing of a two-storey post-tensioned timber building. In Proc., 9th US National and 10th Canadian Conference on Earthquake Engineering, Toronto, Canada; 2010.
13. Mugabo I, Barbosa AR, Sinha A, et al. System identification of UCSD-NHERI shake-table test of two-story structure with cross-laminated timber rocking walls. *J Struct Eng*. 2021;147(4). doi:10.1061/(ASCE)ST.1943-541X.0002938
14. Bhatta J, Dhakal RP, Sullivan TJ. Cyclic Behaviour of two-story low-damage rocking precast concrete cladding panel system. *J Earthquake Eng*. 2022;27:1414-1439. doi:10.1080/13632469.2022.2074918
15. Baird A, Palermo A, Pampanin S, Controlling seismic response using passive energy dissipating cladding connections. In Proc., 2013 NZSEE Conference, Wellington, New Zealand; 2013.
16. Bhatta J, Dhakal RP, Sullivan TJ. Seismic performance of 'rocking' dual-slot track internal partition walls with concealed joints under lateral cyclic drift demands. *J Earthquake Eng*. 2022b:1-26. doi:10.1080/13632469.2022.2112322
17. Magliulo G, Petrone C, Capozzi V, Maddaloni G, Lopez P, Manfredi G. Seismic performance evaluation of plasterboard partitions via shake table tests. *Bull Earthquake Eng*. 2014;12:1657-1677. doi:10.1007/s10518-013-9567-8
18. Petrone C, Magliulo G, Manfredi G. Shake table tests on standard and innovative temporary partition walls: shake table tests on standard and innovative temporary partition walls. *Earthquake Engng Struct Dyn*. 2017;46:1599-1624. doi:10.1002/eqe.2872
19. Yassin A, Ezzeldin M, Wiebe L. Experimental assessment of controlled rocking masonry shear walls without post-tensioning. *J Struct Eng*. 2022;148:04022018. doi:10.1061/(ASCE)ST.1943-541X.0003307
20. Tasligedik AS, Pampanin S. Rocking cantilever clay brick infill wall panels: a novel low damage infill wall system. *J Earthquake Eng*. 2016;21(7):1023-1049.
21. Bianchi S, Pampanin S. Fragility functions for architectural nonstructural components. *J Struct Eng*. 2022;148(10). doi:10.1061/(ASCE)ST.1943-541X.0003352
22. Pampanin S. Emerging solutions for high seismic performance of precast/prestressed concrete buildings. *J Adv Concr Technol*, invited paper for Special Issue on High performance systems. 2005;3(2):207-223.
23. Sarti F, Palermo A, Pampanin S. Fuse-Type external replaceable dissipaters: experimental program and numerical modeling. *J Struct Eng*. 2016;142(12).
24. Dhakal RP, Rashid M, Bhatta J, et al. Shake table tests of multiple non-structural elements in a low – damage structural steel building. In Proc., 4th International Workshop on the Seismic Performance of Non-Structural Elements, Pavia, Italy; 2019.
25. Priestley MJN. Overview of PRESSS research program. *PCI J*. 1991;36(4):50-57.
26. Priestley MJN, Sritharan S, Conley JR, Pampanin S. Preliminary results and conclusions from the PRESSS five-story precast concrete test building. *PCI Journal*. 1999;44(6):42-67.
27. Priestley MJN, Calvi GM, Kowalsky MJ. *Direct Displacement-Based Seismic Design of Structures*. IUSS Press; 2007.
28. Palermo A, Pampanin S, Buchanan AH, Newcombe MP, Seismic design of multi-storey buildings using Laminated Veneer Lumber (LVL). In Proc., 2005 NZSEE Conference, Wairakei, New Zealand; 2005.
29. Ciurlanti J, Bianchi S, Pampanin S, Shake-table tests of a timber-concrete low-damage building: analytical/numerical vs. experimental results. In Proc., 17th World Conference on Earthquake Engineering, Sendai, Japan; 2020.
30. Bianchi S, Ciurlanti J, Perrone D, et al. Shake-table tests of innovative drift-sensitive non-structural elements in a low-damage structural system. *Earthquake Eng Struct Dyn*. 2021;50(9):2398-2420.
31. Endo Y, Roca P. Comparison of similitude laws applied to multi-storey masonry structures with flexible diaphragms. *J Earthquake Eng*. 2022;27:1151-1174. doi:10.1080/13632469.2022.2040655
32. Pampanin S, Marriott D, Palermo A. *New Zealand Concrete Society*. PRESSS Design Handbook; 2010.
33. Priestley NMJ, Calvi GM, Kowalsky MJ. *Direct Displacement-Based Seismic Design of Structures*. IUSS Press; 2007.

34. NTC. *Norme Tecniche per le Costruzioni, Ministero delle Infrastrutture, Supplemento ordinario n°8 alle G.U. n° 42 del 20/02/2018, serie generale*. NTC; 2018.
35. Pampanin S, Palermo AG, Buchanan A. *Structural Timber Innovation Company Inc., Post-Tensioned Timber Buildings – Design Guide*. STIC; 2013.
36. AS/NZS (Standards Australia/Standards New Zealand). *Australian/New Zealand Standard 1170*. AZ/NZS 1170, NZS; 2002.
37. Palermo A, Pampanin S. *Pre-Stressed Beams or Panels (3PT)*. 2017. United States Patent n. US9809979B2 (filed in 2014), Japan Patent n. JP6373975B2 (filed in 2014), Canada Patent n. CA2909402C.
38. NZS1170.5 (Standards New Zealand). *Structural Design Actions – Part 5: Earthquake Actions*. NZS; 2004.
39. Mendes L, Campos Costa A. *LNEC-SPA—Signal Processing and Analysis Tool for Civil Engineers*. LNEC; 2007. Version 1.0, Build 12. Proc. 0305/11/16238. Report 29/2007–NESDE.
40. Pampanin S, Priestley MJN, Sritharan S. Analytical modelling of the seismic behaviour of precast concrete frames designed with ductile connections. *J Earthquake Eng*. 2001;5(3):329-367.

How to cite this article: Pampanin S, Ciurlanti J, Bianchi S, et al. Triaxial shake table testing of an integrated low-damage building system. *Earthquake Engng Struct Dyn*. 2023;1-25. https://doi.org/10.1002/eqe.3906